AD-A061 634 MINNESOTA UNIV MINNEAPOLIS DEPT OF CHEMISTRY F/G 11/6
THE PHYSICAL AND CHEMICAL CHARACTERIZATION OF ELECTROCHEMICALLY--ETC(U)
NOV 78 J F EVANS, M G ALBRECHT, D M ULLEVIG N00014-77-C-0209
UNCLASSIFIED TR-2 NL

1 OF 1
AD
AD61 634

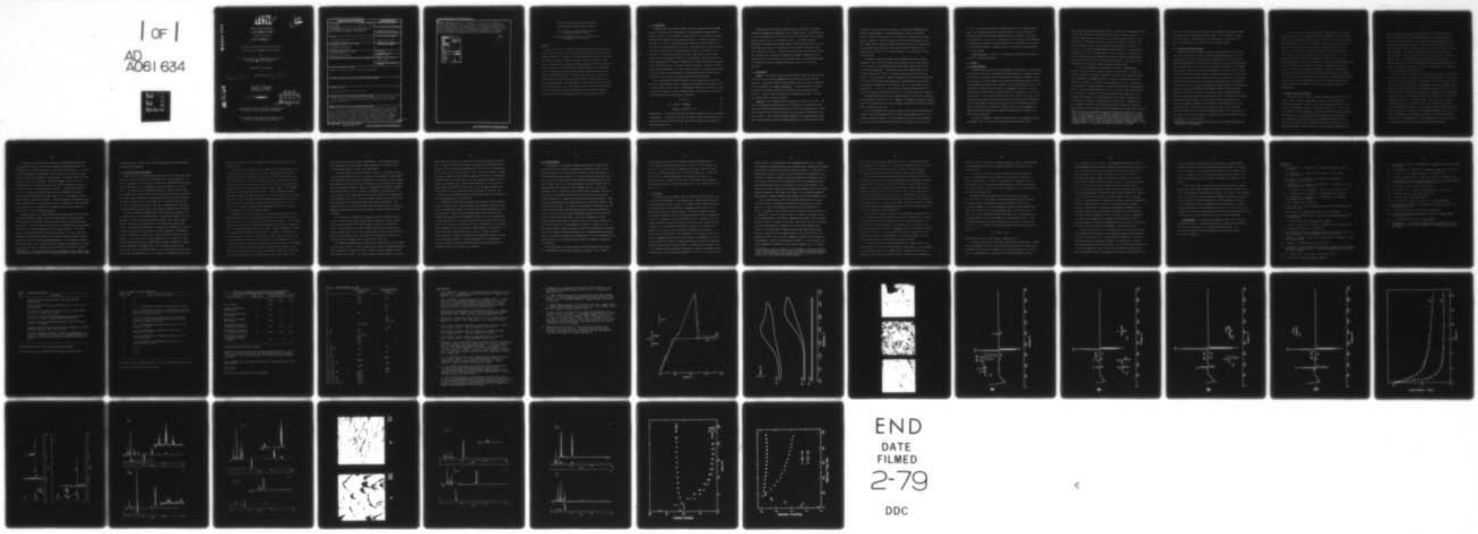

END
DATE
FILMED
2-79
DDC

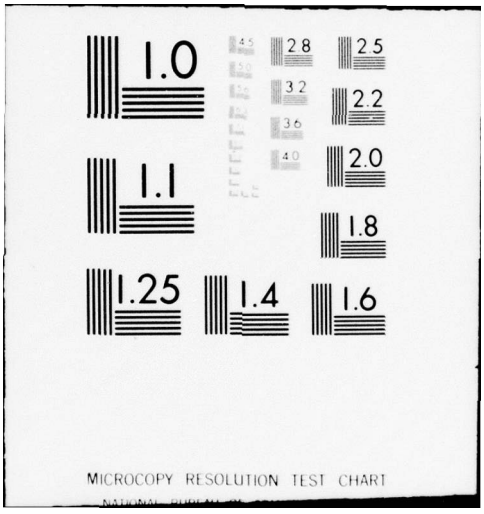
1.0
1.1
1.25
1.4
1.6
1.8
2.0
2.2
2.5
2.8
3.2
3.6
4.0
MICROCOPY RESOLUTION TEST CHART

LEVEL II

12

OFFICE OF NAVAL RESEARCH

(15) Contract N00014-77-C-0209

Task No. NR 051-642

(9) TECHNICAL REPORT NO. 2

(6) The Physical and Chemical Characterization of Electrochemically Reformed Silver Surfaces.

by

(10) John F. Evans, M. Grant Albrecht, Dale M. Ullevig and Robert M. Hexter

Prepared for Publication

in

(12) 48p. Surface Science (14) TR-2

University of Minnesota
Department of Chemistry
Minneapolis, MN 55455

(11) 9 Nov 1978

This document has been approved for public release and sale, its distribution is unlimited

233 515

SECURITY CLASSIFICATION OF THIS PAGE (When Data Entered)

REPORT DOCUMENTATION PAGE		READ INSTRUCTIONS BEFORE COMPLETING FORM
1. REPORT NUMBER NR 051-642	2. GOVT ACCESSION NO.	3. RECIPIENT'S CATALOG NUMBER
4. TITLE (and Subtitle) THE PHYSICAL AND CHEMICAL CHARACTERIZATION OF ELECTROCHEMICALLY REFORMED SILVER SURFACES		5. TYPE OF REPORT & PERIOD COVERED Technical Report No. 2 6. PERFORMING ORG. REPORT NUMBER
7. AUTHOR(s) John F. Evans, M. Grant Albrecht, Dale M. Ullevig, and Robert M. Hexter		8. CONTRACT OR GRANT NUMBER(s) N00014-77-C-0209
9. PERFORMING ORGANIZATION NAME AND ADDRESS The Regents of the University of Minnesota Minneapolis, MN 55455		10. PROGRAM ELEMENT, PROJECT, TASK AREA & WORK UNIT NUMBERS
11. CONTROLLING OFFICE NAME AND ADDRESS Chemistry Program Office of Naval Research Arlington, VA 22217		12. REPORT DATE November 9, 1978 13. NUMBER OF PAGES 45
14. MONITORING AGENCY NAME & ADDRESS(if different from Controlling Office)		15. SECURITY CLASS. (of this report) Unclassified 15a. DECLASSIFICATION/DOWNGRADING SCHEDULE
16. DISTRIBUTION STATEMENT (of this Report) Approved for public release; distribution unlimited		
17. DISTRIBUTION STATEMENT (of the abstract entered in Block 20, if different from Report)		
18. SUPPLEMENTARY NOTES Preprint, submitted to Surface Science		
19. KEY WORDS (Continue on reverse side if necessary and identify by block number) Surfaces, metal, Secondary Ion Mass Spectroscopy, Auger Electron Spectroscopic, Scanning Electron Microscopy, Electrochemistry, enhanced Raman intensity on silver		
20. ABSTRACT (Continue on reverse side if necessary and identify by block number) The effects of electrochemically oxidizing and reducing polycrystalline silver foils in aqueous chloride solutions are studied from a physical and chemical standpoint. Scanning electron microscopy indicates that the resulting surface is extremely rough, consisting of nodular formations. Auger electron spectroscopic, secondary ion mass spectrometric and electrochemical results provide clear indication that a highly purified layer of metallic silver of increased surface area and activity is produced by the electro-		

DD FORM 1 JAN 73 1473 EDITION OF 1 NOV 65 IS OBSOLETE
S/N 0102-LF-014-6601

SECURITY CLASSIFICATION OF THIS PAGE (When Data Entered)

chemical reformation process. No evidence is found for the retention of intense Raman scatterers such as pyridine at these surfaces under ultra-high vacuum conditions. The implications of the chemical and physical state of the reformed silver foils is discussed in the context of theories which have been proposed to explain the anomalously intense spectra of Raman scatterers adsorbed from solution onto these reformed silver surfaces.

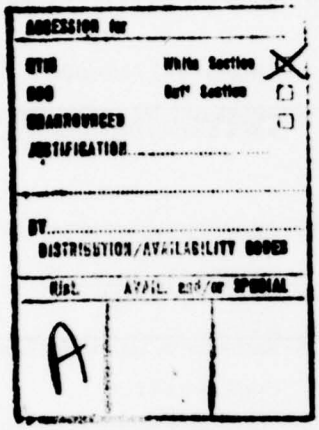

"The Physical and Chemical Characterization of

Electrochemically Reformed Silver Surfaces"

John F. Evans, M. Grant Albrecht, Dale M. Ullevig and Robert M. Hexter

(Department of Chemistry, University of Minnesota, Minneapolis, MN 55455 USA)

Abstract

The effects of electrochemically oxidizing and reducing polycrystalline silver foils in aqueous chloride solutions are studied from a physical and chemical standpoint. Scanning electron microscopy indicates that the resulting surface is extremely rough, consisting of nodular formations. Auger electron spectroscopic, secondary ion mass spectrometric and electrochemical results provide clear indication that a highly purified layer of metallic silver of increased surface area and activity is produced by the electrochemical reformation process. No evidence is found for the retention of intense Raman scatterers such as pyridine at these surfaces under ultra-high vacuum conditions. The implications of the chemical and physical state of the reformed silver foils is discussed in the context of theories which have been proposed to explain the anomalously intense spectra of Raman scatterers adsorbed from solution onto these reformed silver surfaces.

1. Introduction

Recently there have appeared several reports of anomalously intense Raman spectra of molecules and ions adsorbed at electrochemically prepared silver surfaces [1-12]. For the majority of these studies an electrochemical pretreatment has been required to obtain optimal intensity in the Raman spectrum of the adsorbate [1-7, 10-12]. These observations (primarily but not exclusively in the case of pyridine adsorbates) have led to the proposition of several different theories to account for this phenomenon, most of which have assumed that the adsorption of the scattering molecule (or ion) takes place at a pure silver surface of flat topography (relative to the wavelength of exciting radiation). These assumptions have prompted a thorough physical and chemical characterization of such surfaces in order to provide, insofar as possible, a basis for further theoretical considerations. We report here the results of these studies in which we have restricted the investigation to polycrystalline silver foil substrates prepared by electrochemical cycling in aqueous potassium chloride.

The electrochemical procedure consists of first anodizing the surface to generate a silver chloride layer, followed by its reduction, presumably to yield a reformed layer of pure silver. The mechanism by which this reformation process occurs may be summarized by the following sequence of dissolution, complexation, transport and deposition after Katan, et al [13]:

$$Ag \rightleftarrows Ag^{+} + e^{-} \tag{1}$$

$$Ag^{+} + (n+1)Cl^{-} \rightleftarrows AgCl_{(n+1)}^{-n} \tag{2}$$

$$AgCl_{(n+1)}^{-n} \rightleftarrows AgCl(s) + n\ Cl^{-} \tag{3}$$

The sequence 1 - 3 represents the anodization process while the reverse represents cathodization. It should be noted that for either process the dissolution site and deposition site are different and that there is evidence for preferential nucleation sites [13].

Scanning electron microscopic (SEM) studies were carried out to provide information regarding the topography of the reformed surface. Controlled potential electrochemistry has been utilized to probe both the physical and chemical changes associated with the reformation process. The surface sensitive techniques of secondary ion mass spectrometry (SIMS) and Auger electron spectroscopy (AES) were employed to provide more direct chemical information about the reformed silver surface. Depth profiling using both AES and SIMS detection has allowed for the evaluation of variation in elemental composition at the reformed surface, in the "bulk" of the reformed layer, at the interface between the reformed layer and the unmodified substrate, and in the bulk of the substrate.

2. Experimental

Reagents. The solvent used was deionized water further purified by double distillation from potassium permanganate and stored in previously leached glassware. High purity (99.99+%) polycrystalline silver foil was the substrate for all experiments (see Sample Preparation). Potassium chloride, potassium perchlorate and sodium chloride were analytical reagent grade and used as received. Nitrogen, oxygen and argon were ultrahigh purity grade. Pyridine was reagent grade and used as received.

Apparatus. Two ultrahigh vacuum instruments were used in this study. The first, a 3M SIMS spectrometer, was used for recording static SIMS spectra [14] and depth profiles employing SIMS detection, since it was equipped with a rasterable ion gun in which the sputtering gas could be directly introduced into the ion gun source. This allowed for dynamic pumping of the sample chamber during static SIMS experiments using ion pumping augmented by a liquid nitrogen cooled

cryopanel. As such, the partial pressures of residual gas contaminants were minimized during analysis. A second instrument, a Physical Electronics Industries Model 548 ESCA/Auger electron spectrometer equipped with an Extranuclear quadrupole (2-1000 amu range), was used for multi-technique analyses. AES, dynamic SIMS and depth profiling using AES detection were recorded using this instrument which employed a fixed beam, variably focusable ion gun. Sputtering was carried out in a back-filled mode. The sputtering gas was in all cases argon.

Both surface analysis facilities were equipped with signal averaging capability. During all SIMS analyses ion counting was used. Auger spectra were recorded in a non-retarding analyzer mode using analog detection and a 3 eV modulation amplitude. As discussed in the text, minimal power in the focused primary beam (1 KeV at 5 μA target current) was used for most AES analyses. For each sample so analyzed changes in the AES spectra were monitored as a function of electron beam exposure, and AES peak intensity ratios were calculated by extrapolation to zero exposure time. The base pressure for all analyses was $\leq 1 \times 10^{-9}$ torr. This vacuum was attained without bakeout to insure that annealing and diffusion effects in the silver samples were minimized.

Scanning electron microscopy was conducted using a JOEL JEM-100 cx/ASID-4D with an ultimate resolution of 30 Å. Samples to be examined *via* SEM were removed from the electrochemical cell, briefly cleaned ultrasonically in doubly distilled water, and allowed to air dry.

All electrochemistry was carried out using a three electrode potentiostatic system. The electrochemical cell was a closed vessel designed such that the reference electrode (Ag/AgCl, 1.00 *M* KCl) probe was centrally placed normal to the plane of the working (Ag foil) electrode at a distance of *ca* 0.1 *in* from

its face. The platinum auxiliary electrode was located in a separate compartment. This configuration allowed for minimization of lateral variation in applied potential thus promoting optimally uniform film growth. All working electrodes were 1.54 cm^2 in area. Deoxygenation of electrolyte was accomplished by purging nitrogen through the medium pore glass frit separating the auxiliary and electrolysis chambers. Oxygen saturation of electrolyte was accomplished in a similar manner.

Sample Preparation. Tables I and II summarize the details of the preparation of the various sample types.

3. Results

3.1 Electrochemistry

Although controlled potential electrochemistry in the context of the present study has been utilized as a preparative technique employed to generate anodized and reformed silver films, there are several electrochemical observations which are pertinent to the understanding of the physical and chemical nature of these electrochemically modified silver surfaces. From a physical point of view, cyclic voltammetric responses provide a means of estimating the change in electrode capacity (in the double layer potential region) as a consequence of the reformation process. In terms of the chemical nature and activity of the silver film formed by electrochemical cycling procedures, we have found that an examination of the electrochemical current-voltage responses for the reformation process itself in the presence and absence of oxygen, as well as the voltammetry for oxygen reduction at mechanically abraded and reformed silver surfaces, to be particularly informative.

The cyclic voltammetric responses recorded during the reformation process are shown in Fig. 1 for the case of an oxygen-free solution and one in

which the solution was saturated with oxygen (0.3 mM, [15]). Although the curves are virtually identical during the anodization step, a distinct excess of cathodic charge passage is evident in the case where oxygen is present in the electrolyte. Furthermore, the current transient here does not return to zero after the majority of the silver chloride has been reduced to the metal at ca -0.3 V. This result strongly implicates the existence of a chemical oxidation pathway for silver chloride formation which is operative in parallel to the electrochemical process (anodization), and this chemical pathway involves oxygen either directly or in a reduced form such as H_2O_2. This conclusion is substantiated by the various surface analyses discussed below.

The cyclic voltammetry of O_2-saturated 0.1 M KCl at a mechanically abraded silver foil (type A sample, Table 2) is given in Fig. 2, curve B in which the potential excursion is confined to the double layer region (as shown by the background voltammogram, curve A). A broad irreversible wave for the reduction of oxygen[§] is found with a peak potential at -0.55 V. Following the electrochemical reformation process, the peak potential for the oxygen reduction process is shifted anodically (Fig. 2, curve C) to -0.40 V under the same solution conditions. This shift of some 150 mV provides clear indication of the increase in the number of electrocatalytic sites for oxygen reduction on the reformed surface compared to the mechanically abraided foil. Examination of the voltammetric behavior of these same electrodes in oxygen-free solution at higher current sensitivity shows that the charging current on the reformed surface

[§]There is currently considerable disagreement regarding the mechanism of oxygen reduction, particularly as to the number of electrons involved in the initial step. Certain arguments favor the initial monoelectronic reduction of molecular oxygen to form superoxide radical anion ($O_2^{\cdot-}$) which is rapidly protonated and disproportinates to yield hydrogen peroxide and molecular oxygen. Others favor a scheme in which there is direct two electron reduction heterogeneously to yield hydrogen peroxide. For detailed discussions see references [16-19].

is ca 3 - 4 times larger than that found on the mechanically abraded electrode in agreement with the observation of Giles [20]. It is reasonable to assume that this change in charging current arises primarily as a consequence of a much increased surface area in the case of the reformed surface.

3.2 Scanning Electron Microscopy

Scanning electron micrographs at moderate magnification show the reformed surface to be significantly altered during the electrochemical cycle (Fig. 3). The reformed silver surface is composed of nodular deposits [13,17,21] which grow three-dimensionally [13,20] during the reduction of the anodically generated silver chloride film. At low values of charge passed (50 mC/cm^2), the reformed silver does not completely cover the foil substrate as shown in Fig. 3A. While a calculation based on the bulk density of silver would lead one to predict such a layer to be ca 500 Å thick if uniform lateral growth prevailed, it is apparent from the above micrograph that the growth of the reformed layer has proceeded at preferred sites in a non-uniform manner with nodule heights and lateral spacing ranging from ca 6000 to 10,000 Å. When higher amounts of charge are passed (500 mC/cm^2, Fig. 3B) the nodule size appears to remain relatively constant, while the gross spacing between the nodules decreases to ca 3000 Å on the average. At higher magnification (Fig. 3C) inter-nodule clefts and boundaries [13] become more apparent, suggestive of the growth of nodules both on top of and into one another. These clefts are on the order of 50 - 100 Å across, and they may be involved in the capillary condensation model recently proposed [22] to account for the observed potential step Raman spectroelectrochemistry [6] of pyridine at this reformed surface.[§]

[§] Small pores of diameters less than the resolution of the SEM (<30 Å) may also contribute to this phenomenon.

It should be noted that when even thicker layers (7500 mC/cm^2 of charge passage) are subjected to prolonged ultrasonic treatment (3 - 4 h) in water, some of the nodules become separate from one another and are physically shaken from the surface, the smaller ones forming relatively stable colloidal suspensions. Since this was not the case for the thinner reformed surfaces (50 mC/cm^2), it is proposed that the inter-nodular clefts are quite deep. In no cases were crystallites observable in the reformed layer [13]. It is conceivable that minute dendrites or needles were present initially on the nodules immediately after their formation, but that either during removal from the electrochemical cell, transfer to the SEM or examination via SEM this structure collapsed to that which is observed. However, we stress that if such surface structures do exist and collapse when the surface is disturbed, they are apparently not required for the observation of enhanced Raman scattering intensities from adsorbed molecules, since the reformed surface may be removed from the electrochemical cell and still exhibit the enhancement phenomenon [7].

3.3 Auger Electron Spectroscopy

The AES spectrum of a freshly prepared, mechanically abraded silver foil (Fig. 4) shows relatively high levels of sulfur-, chlorine- and oxygen-containing contaminates as well as trace carbon contaminates levels, all of which can be completely removed by brief argon ion etching. If such a foil is subjected to the electrochemical reformation process and rinsed with water, high levels of KCl contamination from the electrolyte are noted (Fig. 5). The reformation procedure also results in considerable diminution of the surface oxygen content and near-elimination of carbon contaminates. If an analogously prepared reformed surface is briefly washed ultrasonically in

water to remove residual KCl, the AES spectrum of the resulting surface (Fig. 6) indicates that the KCl deposits have been efficiently removed by this procedure. We therefore conclude that the KCl was probably trapped in the porous network discussed above. There still remains, however, a high level of surface chlorine, probably in the form of AgCl (see below). Surface oxygen content is also noted to decrease to a nearly undetectable level after ultrasonic washing, indicating that the previously observed oxygen contaminate (Fig. 5) is predominantly water retained in the KCl deposits. It should be noted that the sulfur containing contaminates always observed on the mechanically abraded surface (Fig. 4) have been eliminated as a consequence of the electrochemical reformation cycle.

It was of interest to compare the AES peak-to-peak intensity ratios found for bulk silver chloride to those found for the residual AgCl on the reformed surfaces, such that an estimate of the thickness of the silver chloride film in the latter case might be made. In attempting to obtain a standard reference spectrum of silver chloride formed anodically in aqueous KCl (Fig. 7) it was noted that electron beam damage was prevalent. Consequently, the primary beam energy and current density were reduced for AES analyses and all samples were repetitively analyzed as a function of time. Such a procedure for thick (ca 5000 Å) AgCl films is compared in Fig. 8 to a depth profile obtained using 1 KeV argon ion etching. It is clear that although a steady state Cl/Ag ratio is attained more rapidly in the ion-bombarded example (curve A), this ratio is approached when the sample is subjected to electron beam exposure alone (curve B). Extrapolation of either damage profile to zero time permits an accurate evaluation of the AES peak-to-peak intensity ratios.

The presence of a high chloride level on the reformed silver surface was not anticipated, and as a consequence considerable attention was given to the determination of possible sources of the AgCl found on the surfaces. The results of these experiments are summarized in Table 3 where the AES intensity ratios have been corrected for damage as discussed above. No elements other than those listed in Table 3 were detectable. These data suggest that the source of residual AgCl on the reformed surfaces arises from the simultaneous exposure of silver surfaces to oxygen and aqueous chloride. (Compare sample types G-I with J, K.) Although the residual AgCl level was suppressed by excluding oxygen during the preparation of sample types G and J, the formation of some AgCl could not be completely prevented. The electrochemical reformation process is not prerequisite to the observation of AgCl, and therefore it must be assumed that the AgCl is not a consequence of incomplete charge recovery during the reduction step of the reformation procedure.

Hydrogen peroxide is a significantly more effective oxidant for silver than is dissolved molecular oxygen, since the Cl/Ag intensity ratio for peroxide treated samples is essentially the same as that found for the anodically grown AgCl control. Both this control and the peroxide treated sample are exceptionally clean--silver and chlorine being the only detectable elements. On the other hand, it should be noted that although AgCl is formed to a certain extent when mechanically abraided silver surfaces are exposed to aqueous chloride solution, significant sulfur and carbon contamination persist. More prolonged ultrasonic treatment of these foils in chloride solution saturated with oxygen did not yield lower sulfur and carbon contaminate levels, and this may indicate[§] that these

[§]Unfortunately, the gross difference in surface topography does not permit a meaningful quantitative comparison of the Cl/Ag ratios found for these surface types.

contaminates protect certain silver sites from oxidation by molecular oxygen followed by AgCl formation.

3.4 Secondary Ion Mass Spectrometry

Owing to its vastly increased sensitivity over AES, the SIMS technique was utilized to further characterize the reformed silver electrode surfaces. In order to facilitate the presentation of positive ion SIMS (POSSIMS) and negative ion SIMS (NEGSIMS) data, the appropriate m/e peak assignments are given in Table 4. The SIMS results are generally supportive of those obtained using AES, although trace levels of species not detected by AES are readily observed using SIMS. While examination of the various surfaces by the SIMS technique was easily carried out in the static mode [14], it was found that the low ion yields for subsurface regions of either the reformed layer or bulk silver foil required higher primary beam current densities (dynamic SIMS conditions).

The static POSSIMS and NEGSIMS spectra of an anodically grown AgCl film are shown in Figs. 9A and 9B, respectively. These spectra indicate that trace impurities of sodium, aluminum, potassium, chromium, iron, copper, oxygen, fluorine and bromine are present on the electrochemically generated AgCl surface. Hydrocarbon contamination is low and sulfur contaminates, if present, are below detectable levels in contrast to their prominence in the NEGSIMS spectra of mechanically abraded foils. $AgCl^+$ and Ag_2Cl^+ clusters are readily observed. On the other hand, clusters indicative of the formation of silver oxides during anodization (e.g., $AgOH^+$ which is readily observed at 0.2 times the Ag^+ peak height in POSSIMS spectra of foils anodized in aqueous perchlorate solutions) are distinctly absent. It is interesting to note the presence of peaks corresponding to the Cl_2^- species in the NEGSIMS spectrum, since

this species must arise from a recombination or rearrangement process during sputtering [23].

A sample which was subjected to both anodization and cathodization, but not ultrasonically cleaned in water prior to static SIMS, showed the anticipated (from AES) high levels of clusters such as K_2^+, K_2Cl^+, KAg^+ and $KAgCl^+$ in the positive ion spectrum (Fig. 10A). Analogous species were observed with sodium replacing potassium in these clusters when the electrolyte was aqueous sodium chloride instead of the potassium salt (type F sample, Table 2). The NEGSIMS spectrum (Fig. 10B) indicates lower levels of fluorine contaminate, higher hydrocarbon content and bromine is present at a level nearly two orders of magnitude higher than on the sample which had undergone anodization only. Several unique clusters are observed in the negative ion spectrum as well, such as $ClBr^-$, KCl_2^- and $AgCN^-$. Similar POSSIMS and NEGSIMS spectra were recorded for a KCl-contaminated foil (type B sample, Table 2).

Reformed silver surfaces subjected to ultrasonic cleaning prior to static SIMS analysis yield spectra which are quite different from those observed for samples which were not cleaned in this fashion prior to analysis. In the POSSIMS spectrum (Fig. 11A) the potassium peak is diminished by two orders of magnitude and the potassium-containing clusters are absent. Copper contamination is found to be notably higher; indeed, an $AgCu^+$ cluster is detected. Presumably this contaminate has its source either in the water or the electrolyte or both, and is electrodeposited during the cathodic sweep of the electrochemical cycle. The presence of AgCl is noted by the appearance of Ag_2Cl^+ clusters in the POSSIMS sectrum. The primary distinction between the negative ion spectrum for this sample (Fig. 11B) and the previous case (no ultrasonic wash) is the significant reduction in the intensity of the bromine peaks. This result points to the

electrolyte as the source of bromide contamination. Chlorine peaks dominate the NEGSIMS spectrum of this sample, again confirming the existence of AgCl on the reformed surfaces as noted in the AES analyses.

In that one purpose for undertaking this study was to chemically characterize the reformed silver surface as it relates to the anomalously intense Raman scattering intensities for solution adsorbates such as pyridine, several samples were prepared in which pyridine was incorporated in the electrolyte used during the electrochemical treatment. Under no circumstances were NEGSIMS or POSSIMS peaks detected which could be attributed to pyridine or silver-pyridine complexes analogous to the argentated species recently reported for p-aminobenzoic acid adsorbed on silver [24]. Moreover, dosing of sputter-cleaned silver foils with pyridine in the SIMS apparatus also did not yield such species. This suggests that the interaction of pyridine with silver metal is due to physical adsorption, which allows for the facile removal of surface pyridine under UHV conditions.

For the purpose of comparing the composition of the reformed layer with that of the bulk foil precursor, dynamic SIMS conditions (7.5 $\mu A/cm^2$ primary ion beam current density) were required owing to drastically reduced ion yields. This reduction in ion yield (and most likely sputter yield) has two possible origins [25]. The first is the diminution in the silver surface sites which are in an oxidized form. The second is the formation of cones during sputtering into the reformed layer or the bulk foil (Fig. 12).

The POSSIMS and NEGSIMS spectra observed after sputtering into the reformed layer are given in Figs. 13A and 13B, respectively, and the corresponding spectra for the bulk foil are Figs. 14A and 14B. There are several important distinctions between the two cases. For the CN^- species the peak intensity is ca three

times larger in the bulk foil. While sulfur is readily observed in the bulk foil, it cannot be noted in the negative ion spectrum of the reformed layer. The m/e 27 peak in the positive ion spectrum (Al^+ or $C_2H_3^+$) is notably higher in the case of the foil (ca a factor of four). With the exception of sodium, potassium, chromium, iron and fluorine, which are found to be at approximately the same level in both sample types, all other species show higher intensity peaks in the reformed layer. These include oxygen and C_2^- at ca twice the levels found in the bulk; Cu^+, Ag^+ and Cl^- at ca ten times that observed in the bulk and Br^- at ca a thirty-fold higher level than in the bulk. Ag_2^+ is detectable in the POSSIMS spectrum of the reformed layer, but is absent in the corresponding data for the bulk foil.

In summary, the SIMS results confirm the AES analyses, and they provide further indication (due to the sensitivity of the technique) that the electrochemical reformation procedure is extremely effective in purifying the silver foil electrodes. Those surface contaminates which are detectable on the reformed layer via SIMS are attributable to either trace solution impurities or silver halides which result from the interaction of oxygen with the silver surface in the presence of soluble halide ions. Furthermore, it is suspected that the members of this latter group of surface species are not likely to be present when the reformed electrodes are poised at cathodic potentials, except possibly at extremely low steady state coverage when oxygen is present in the electrolyte solution. Of primary importance is the elimination of sulfide and cyanide surface species which would block the physisorption of the Raman scatterers of interest, e.g., pyridine.

3.5 Depth Profiling

To determine if the presence of high concentrations of oxygen in the electrolyte solution during the reformation procedure gives rise to a substantially higher level of surface AgCl compared to cases where oxygen is excluded from the solution (see Sec. 3.1), depth profiles using AES detection were carried out on samples which were reformed in deoxygenated aqueous KCl (type G sample, Table 2), air-saturated aqueous KCl (type H sample, Table 2) and oxygen-saturated aqueous KCl (type I sample, Table 2). The results presented in Fig. 15 show that in all cases the AgCl is primarily confined to the surface of the nodular reformed silver layer, with the chlorine peak rapidly decreasing to a relatively low level as the profiling proceeds. From the results presented here, we cannot definitively identify the source of this residual chlorine signal. It could arise from chlorine recombination with the silver during sputtering; chlorine being knocked in during sputtering; the surfaces of pores, voids and channels being uncovered during the sputtering of such a rough surface (see Figs. 3 and 12); or a combination of these. Although identical profiles are found for silver in the various sample types, the chlorine profiles are differentiable on the basis of whether or not a high concentration of oxygen was present during the electrochemical reformation cycle (air or oxygen saturated conditions) or not (deoxygenated with nitrogen). When the electrolyte was purged with nitrogen prior to the electrochemical cycle, the initial level of the chlorine signal is lower and remains so during the entire profile.

One trace species, the concentration of which is significantly reduced as a consequence of the reformation process, is cyanide. Fig. 16 shows a

NEGSIMS depth profile across the interface (albeit ill-defined) of the reformed layer and the bulk silver foil for the m/e = 24 and 26 peaks. The former (C_2^-) is seen to grow to a maximum at the apparent interface and then diminish as sputtering proceeds into the bulk foil substrate. On the other hand, the m/e = 26 peak (predominately CN^-) grows as the interface is approached, and it is nearly constant after the interface has been passed. The slight decrease in this peak is indicative of a $C_2H_2^-$ hydrocarbon contribution to it.

4. Discussion

The foregoing results indicate that the electrochemical reformation procedure which is prerequisite to the observation of enhanced Raman scattering of adsorbed species yields a surface of increased activity (both with respect to adsorption and electron transfer) of spongelike silver which is of much higher purity than the precursor surface. The surface analytical results show unquestionably that sulfur and cyanide contaminate levels are drastically reduced as a consequence of the electrochemical cycle. Although copper contamination appears to take place during the cathodic step of this cycle (as a consequence of electrodeposition from the electrolyte), the level of this impurity is very low and could probably be eliminated by electrolytic purification of the solution. The determination of the degree of purity with respect to anionic solution species which readily form insoluble silver salts (e.g., chloride and bromide) is complicated by the ease with which oxygen and hydrogen peroxide oxidize metallic silver. It should be noted, however, that at the cathodic potentials employed to maximize or modulate the Raman intensity enhancement in the use of pyridine adsorbate [5-7,10,11], these silver salts are

readily reduced to silver metal and the corresponding halide ion. As such, in the absence of dissolved oxygen, AgCl and AgBr surface impurities (if present) are completely depleted with an applied negative potential. In cases where an oxidant such as oxygen or hydrogen peroxide (formed as an intermediate in the reduction of oxygen) is present in solution following the reformation process, the reaction of these molecules with metallic silver at cathodically poised potentials would not lead to the formation of surface silver halide[§]. The observation of silver halide on electrochemically reformed silver by the surface analysis techniques is then simply an artifact of the coincident exposure of these samples to aqueous chloride during removal from the electrochemical cell.

From a chemical point of view, the reforming process serves to purify the silver surface, thus making the adsorption of any molecule or ion more facile (i.e., more active adsorption sites per unit electrode area are formed). In addition, from a physical point of view, the total electrode area is increased by a factor of three or four, as a result of the nodular nature of the reformed silver. The surface roughness which results from the electrochemical reduction is therefore quite high. This view of the surface provided by surface spectroscopy and scanning electron microscopy supports those theories of the enhancement of Raman scattering from these surfaces which invoke the coupling of surface plasmon states to the excited states of the adsorbates [26,27], just as surface roughness is required for the coupling of electromagnetic radiation to these states [26,28,29]. In these theories, the surface roughness is required to have a Fourier component at $k = \lambda^{-1}$, where λ

[§] If one chooses to think of the product of the chemical oxidation of metallic silver as intermediate Ag^+ surface states, then these are certainly reduced by current flow to the surface more rapidly than they can react with solvated halide ions at the electrode-electrolyte interface.

is the excitation wavelength. This implies that the reformed silver surface should appear to be colored, as the excitation wavelengths which have been used are in the visible region of the spectrum. Indeed, the electrochemically reformed silver surfaces described above have a creamy yellow appearance.

On the other hand, mechanical abrading [8,9,12] or inherent roughness of vapor-deposited silver films [30] have apparently provided sufficient roughness in experiments on adsorbed CN^- and CO, respectively. Using electrochemical roughening, Pettinger and Wenning have found that the relative Raman intensity increases monotonically to a factor of greater than 10^3 as the total charge transferred is increased over the range 0.03 - 10 monolayers of silver [10]. We have already described the microscopic changes in the surface that accompanies this increase (Fig. 3). As far as we are aware, there is no theory of the Raman enhancement in which this quantitative dependence of the scattered intensity on the surface roughness has been accounted for.

There has been one theory proposed for the anomalously high Raman intensities in one system which does not require any surface roughness [6]. According to this theory, specific ion adsorption occurs in a layer intermediate to the metal and the scattering adsorbate. The anomalous scattering intensity has then been qualitatively ascribed to a chemical interaction between the adsorbate and the ionic layer, i.e., the electronic structure of the adsorbate is modified so as to increase the Raman intensity. This theory, however, does not account quantitatively for the observed intensity enhancement.

The surface spectroscopic studies reported here, however, show that the reformed silver is in a state of extraordinary chemical purity. It is primarily a silver surface, quite free of oxygen, sulfur, cyanide and other typical impurities. Some chloride is present as AgCl, resulting from the simultaneous

exposure of the silver surface to oxygen and aqueous chloride. Moreover, depth profiling shows that the AgCl is primarily confined to the surface of the reformed silver.

If any surface chloride is present, however, consideration should be given to the possibility that the adsorbed Cl^- may itself inelastically scatter radiation (i.e., as AgCl). This possibility is important since all Raman studies of electrochemically reformed silver have noted the appearance of a line at $\sim$240 cm^{-1}, which is not due to pyridine, as it is easily detected when pyridine is absent [11].

The infrared absorption spectrum of solid AgCl has its maximum at 103 cm^{-1} [31]. As is well known, the observed transverse optical (TO) mode of the AgCl crystal (which has the rock salt structure) is the sum of a mechanical frequency ω_o and an electromagnetic (dipole-dipole) coupling term, which shifts and splits the triply degenerate (F_{1u}) optical branch at $\underset{\sim}{k} \cong 0$ into the TO and the longitudinal optical (LO) mode [32]. The coupling can be calculated exactly, and it can be shown to be approximately 114 cm^{-1}. From the observed frequency and these calculations, ω_o is found to have the value of 81 cm^{-1}. ω_o is related to the nearest-neighbor Ag-Cl stretching force constant, f, by

$$\omega_o^2 = 2f(M^{-1} + m^{-1})$$

where M and m are the Ag and Cl masses, respectively [33].

The Ag-Cl stretching force constant, together with the dipole-diple coupling that occurs within one layer of AgCl, can be used to calculate a "single layer frequency," which can then be compared to the observed Raman line at $\sim$240 cm^{-1} [34]. In this calculation, the image effects first discussed by Delanaye,

Lucas and Mahan [35] were utilized. The intrinsic dipole moment as well as the induced moment due to both the externally applied field and the field produced at the source molecule by the dipoles of all other molecules in the lattice (adsorbed layer + image) were included. The result is that the calculated vibrational frequency of a AgCl layer, taking into account both dipole-dipole coupling and image effects, is 140 cm^{-1}. The calculation makes use of an effective ionic charge (dipole derivative) for AgCl equal to 51.2 esu $g^{-\frac{1}{2}}$, which was derived by Jones, et al from dielectric dispersion and infrared transmission experiments on thin crystals of AgCl [31]. However, if the effective charge for AgCl in a monolayer were $\sqrt{2}$ that in the bulk crystal, the calculated Raman frequency for a monolayer would be approximately 200 cm^{-1}. Agreement within a factor of $2^{\frac{1}{2}}$ with the effective charge as determined from dielectric dispersion and transmission experiments on the bulk AgCl crystal in the far infrared is reasonable, and we are therefore inclined to assign the observed 240 cm^{-1} line as due to AgCl. Furthermore, in a study of CN^- adsorbed on Ag, a Raman line was observed at 226 cm^{-1}, which was assigned to the Ag-C stretching mode [12]. Because of the chemical similarity of AgCl and AgCN, this assignment is probably also correct.

The ease with which trace Cl^- and adsorbed CN^- can be detected by Raman spectroscopy is another example of the intensity enhancement phenomenon which occurs at a metal surface [27]. The detection of adsorbed Cl^- on silver by Raman spectroscopy is significant because it was carried out on a surface that was well-characterized by AES and SIMS. The fact that trace ions can thus be detected in situ, on a metal in contact with aqueous electrolyte, gives Raman spectroscopy a number of advantages over all particle spectroscopies, in

which the sample must be withdrawn from the electrolyte, washed and dried thoroughly, and then studied under ultrahigh vacuum conditions. In carrying out these operations, it is possible if not probable that the nature of the surface is changed. None of the particle spectroscopies can directly yield structural information, and all of them are damaging to the sample in some respect.

In this study, however, the particle spectroscopies used were of great value, in that they enabled independent chemical and physical characterization of the electrochemically reformed silver surfaces. As a result of the combined study of this surface using both particle and Raman spectroscopy, we have been able to show that this particular surface is of extraordinary cleanliness. The only significant surface contaminate has been shown to be Cl^-, and the in situ observation of a strong Raman line at 240 cm^{-1} ($\sim 5 \times 10^4$ counts/sec) on a polycrystalline silver surface which has simply been etched in aqueous KCl [11], is consistent with these determinations, and is a notable achievement.

Acknowledgments. This research was supported in part by the Office of Naval Research, the U. S. Army Research Office, the Donors of the Petroleum Research Fund, administered by the American Chemical Society, the International Business Machines Corporation, and the Graduate School, University of Minnesota.

References

1. M. Fleischmann, P. J. Hendra and A. J. McQuillan, Chem. Phys. Lett. 26 (1974) 163.

2. A. J. McQuillan, P. J. Hendra and M. Fleischmann, J. Electroanal. Chem. 65 (1975) 933.

3. R. L. Paul, A. J. McQuillan, P. J. Hendra and M. Fleischmann, J. Electroanal. Chem. 66 (1975) 248.

4. M. Fleischmann, P. J. Hendra, A. J. McQuillan, R. L. Paul and E. S. Reid, J. Raman Spectroscopy 4 (1976) 269.

5. M. G. Albrecht and J. A. Creighton, J. Am. Chem. Soc. 99 (1977) 5215.

6. D. L. Jeanmaire and R. P. VanDuyne, J. Electroanal. Chem. 84 (1977) 1.

7. J. A. Creighton, M. G. Albrecht, R. E. Hester and J. A. D. Matthew, Chem. Phys. Lett. 55 (1978) 55.

8. A. Otto, Surface Sci. 75 (1978) 392.

9. A. Otto, Proc. Int. Conf. on Vibrational Spectroscopy of Adsorbed Layers, Jülich, June, 1978.

10. B. Pettinger and U. Wenning, Chem. Phys. Lett. 56 (1978) 253.

11. B. Pettinger, U. Wenning and D. M. Kolb, Berichte der Bunsengesellschaft, to be published.

12. T. E. Furtak, Solid State Communications, submitted.

13. T. Katan, S. Szpak and D. N. Bennion, J. Electrochem. Soc. 121 (1974) 757.

14. A. Benninghoven, Surface Sci. 35 (1973) 427.

15. W. F. Linke, *Solubilities of Inorganic and Metal Organic Compounds*, Vol. II (American Chemical Society, Washington, D.C., U.S.A., 1965).

16. D. Behar, G. Czapski, J. Rabini, L. M. Dorfman and H. A. Schwartz, J. Phys. Chem. 74 (1970) 3209.

17. I. Morcos, J. Electrochem. Soc. 122 (1975) 1008.

18. E. Yeager, in: *Electrocatalysis on Non-Metallic Surfaces*, Ed. A. D. Franklin (NBS Special Publication 455, U.S. Government Printing Office, Washington, D.C., U.S.A., 1976).

19. D. T. Sawyer and E. T. Seo, Inorg. Chem. 16 (1977) 499.

20. R. D. Giles, J. Electroanal. Chem. 27 (1970) 11.

21. H. Gu and D. N. Bennion, J. Electrochem. Soc. 124 (1977) 1364 and references cited therein.

22. M. G. Albrecht, J. F. Evans and J. A. Creighton, Surface Sci. 75 (1978) 777.

23. J. A. Taylor and J. W. Rabalais, Surface Sci. 74 (1978) 229.

24. H. Grade, N. Winograd and R. G. Cooks, J. Am. Chem. Soc. 99 (1977) 7725.

25. G. K. Wehner, in: *Methods of Surface Analysis*; Ed. A. W. Czanderna (Elsevier Scientific Publishing Co., Amsterdam, 1976), pp. 5 - 37.

26. M. R. Philpott, J. Chem. Phys. 62 (1975) 1812.

27. R. M. Hexter and M. G. Albrecht, Spectrochim. Acta A, 1978, in press.

28. H. Raether, Physics of Thin Films 9 (1977) 145.

29. H. Raether, Nuovo Cimento 39B (1977) 817.

30. T. H. Wood and M. V. Klein, J. Vac. Sci. Tech. March/April (1979).

31. G. O. Jones, D. H. Martin, P. A. Mawer and C. H. Perry, Proc. Roy. Soc. (London) A261 (1961) 10.

32. D. Fox and R. M. Hexter, J. Chem. Phys. 41 (1964) 1125.

33. G. Turrell, "Infrared and Raman Spectra of Crystals" (Academic Press, New York, 1972) p. 186.

34. H. F. Nichols and R. M. Hexter, to be published.

35. F. Delanaye, A. A. Lucas and G. D. Mahan, Proc. 7th Intern. Vac. Congr. & 3rd Intern. Conf. Solid Surfaces (Vienna, 1977) R. Dobrozemsky, et al, eds., pp. 477-480.

TABLE 1. *Preparative Procedures*

Step	Description
1	Mechanical abrasion with grit number 320A, then number 600 abrasive paper.
2	Ultrasonic cleaning in doubly distilled water for 15 min., twice; then air dried.
3	KCl exposure (to provide a KCl covered surface) by twice dipping in 0.1 M KCl followed by air drying.
4	Controlled potential anodization *via* linear sweep from -0.550 V to +0.200 V at 1 mV/s[a]. (Charge passed *ca* 500 mC/cm^2)[b]
5	Controlled potential cathodization *via* linear sweep from +0.200 V to -0.5[illegible] V at 1 mV/s[a].
6	Immediate washing with doubly distilled water followed by ultrasonic cleaning in same for 5 min., then air dried.
7	Ultrasonic treatment for 15 min. in either (a) deoxygenated 0.1 M KCl, (b) O_2 saturated 0.1 M KCl or (c) air saturated 0.1 M KCl containing *ca* 2 x 10^{-4} M H_2O_2; followed by ultrasonic cleaning as in b above.

[a] Solution conditions were varied, and are described in Table 2.

[b] Thick reformed layers were employed unless otherwise noted (see text).

Table 2. Summary of Sample Preparation

Sample Type[a]	Sample Preparation Sequence[b]
A	1-2
B	1-3
C	1-2, 4, 6; anodization carried out in deoxygenated 0.1 M KCl.
D	1-2, 4, 6; anodization carried out in deoxygenated 0.1 M $KClO_4$, anodic potential limit was +0.400 V, after sweep potential was held at this limit for 30 min.
E	1-2, 4-5; anodization and cathodization carried out in air saturated 0.1 M KCl, washed with doubly distilled water (no ultrasonic treatment), air dried.
F	1-2, 4-5; anodization and cathodization carried out in air-saturated 0.1 M NaCl.
G	1-2, 4-6; anodization and cathodization carried out in deoxygenated 0.1 M KCl.
H	1-2, 4-6; anodization and cathodization carried out in air-saturated 0.1 M KCl.
I	1-2, 4-6; anodization and cathodization carried out in oxygen-saturated 0.1 M KCl.
J	1-2, 7a
K	1-2, 7b
L	1-2, 7c

[a] In general at least 2 samples (typically 4-5) of each type were characterized.

[b] Preparative procedures are given in Table 1.

Table 3. Comparison of AES peak-to-peak intensity ratios extrapolated to zero electron beam exposure time for various preparations

Surface Description	Sample Type[a]	Average AES Intensity Ratios[b]		
		Cl/Ag	S/Ag	C/Ag[c]
Silver chloride	C	1.98	d	d
Reformed in oxygen-free KCl solution	G	0.27	d	e
Reformed in air-saturated KCl solution	H	0.39	d	e
Reformed in O_2-saturated KCl solution	I	0.40	d	e
Ultrasonically treated in oxygen-free KCl solution	J	0.32	0.22	0.28
Ultrasonically treated in O_2-saturated KCl solution	K	0.41	0.25	0.16
Ultrasonically treated in KCl solution containing 0.2 mM H_2O_2	L	1.94	d	d

[a] Sample preparations detailed in Table 2.

[b] Ratios are from peak-to-peak height for the following transitions: S-150 eV, Cl-150 eV, C-270 eV and Ag-350 eV. All analyses carried out at a primary beam energy of 1 KeV and a beam current of 5 μA with the analyzer modulated at 3 eV.

[c] Where possible C was quantitated by correction for overlap with the Ag transition at 266 eV.

[d] Not detected.

[e] Trace detected, intensity too low to quantitate.

Table 4. Peak Assignments for SIMS

m/c	Positively Charged Species	Negatively Charged Species
12	C^+	C^-
13	CH^+	CH^-
14	CH_2^+	
16		O^-
17		OH^-
19		F^-
23	Na^+	
24		C_2^-
25		C_2H^-
26		$C_2H_2^-$, CN^-
27	Al^+, $C_2H_3^+$	
32		S^-, O_2^-
35, 37	Cl^+	Cl^-
39, 41	K^+	
40	Ca^+, Ar^+	
52	$^{52}Cr^+$	
56	$^{56}Fe^+$	
63, 65	Ca^+	
70, 72, 74		Cl_2^-
78, 80, 82	K_2^+	
79, 81		Br^-
107, 109	Ag^+	
109, 111		$^{39}KCl_2^-$
113, 115	$^{39}K_2Cl^+$	
114, 116, 118		$ClBr^-$
124, 126	$AgOH^+$	
133, 135		$AgCN^-$
142, 144, 146	$AgCl^+$	$AgCl^-$
146, 148	$^{39}KAg^+$	
181, 183, 185	$^{39}KAgCl^+$	
214, 216, 218	Ag_2^+	
249, 251, 253, 255	Ag_2Cl^+	

Figure Captions

1. Cyclic voltammetric response for the reformation cycle carried out in 0.1 M aqueous KCl: A - deoxygenated solution (N_2 purge) and B - oxygen-saturated solution. Scan rate was 1 mV/s.

2. Cyclic voltammetry for oxygen reduction to 0.1 M aqueous KCl: A - oxygen-free solution at mechanically abraded silver foil (type A surface, see Table 2), B - oxygen-saturated solution at same electrode, C - oxygen-saturated solution at electrochemically reformed silver surface (type G surface, see Table 2). Scan rate in all cases was 50 mV/s.

3. Scanning electron micrographs of reformed silver surfaces: A - 50 mC/cm^2 charge passed, magnification x 10^4; B - 500 mC/cm^2 charge passed, magnification x 10^4; and C - 500 mC/cm^2 charge passed, magnification x 10^5.

4. AES spectrum of mechanically abraded silver foil (type A sample, Table 2). Primary beam voltage: 3 KeV, beam current: 20 μA, analyzer modulation: 3 eV.

5. AES spectrum of reformed silver foil not subjected to ultrasonic cleaning (type E sample, Table 2). Analysis parameters as for Fig. 4.

6. AES spectrum of reformed silver foil subjected to ultrasonic cleaning (type H sample, Table 2). Analysis parameters as for Fig. 4.

7. AES spectrum of silver chloride film grown anodically of silver foil (type C sample, Table 2). Analysis parameters as for Fig. 4.

8. Comparison of electron beam and argon ion beam damage incurred by anodically grown silver chloride film (type C sample, Table 2). Curve A - AES analysis during ion bombardment; AES primary beam energy: 1 KeV, primary beam current: 5 μA, analyzer modulation: 3 eV; Ar^+ ion beam energy: 1 KeV, ion current density: 30 $\mu A/cm^2$. Curve B - as curve A without ion bombardment. Ag and Cl peak-to-peak intensity measured for transitions at 350 and 180 eV, respectively.

9. A: Static POSSIMS spectrum of silver foil anodized in aqueous KCl solution (type C sample, Table 2). B: Static NEGSIMS spectrum of silver foil anodized in aqueous KCl solution (type C sample, Table 2). Analysis conditions: primary ion beam -1 KeV argon at 15 nA/cm^2.

10. A: Static POSSIMS spectrum of electrochemically reformed silver surface (aqueous KCl) not washed ultrasonically (type E sample, Table 2).
b: Static NEGSIMS spectrum of electrochemically reformed silver surface (aqueous KCl) not washed ultrasonically (type E sample, Table 2). Analysis conditions identical to those of Fig. 9.

11. A: Static POSSIMS spectrum of electrochemically reformed silver surface (aqueous KCl) ultrasonically washed after preparation (type H sample, Table 2).
B: Static NEGSIMS spectrum of electrochemically reformed silver surface (aqueous KCl) ultrasonically washed after preparation (type H sample, Table 2). Analysis conditions identical to those of Fig. 9.

12. Scanning electron micrographs of ion bombarded silver surfaces: A - in the reformed silver layer, magnification 2 x 10^4; B - in the bulk foil, magnification x 10^3.

13. A: Dynamic POSSIMS spectrum in the reformed silver layer (type H sample, Table 2). B: Dynamic NEGSIMS spectrum in the reformed silver layer (type H sample, Table 2). Analysis conditions: primary ion beam -1 KeV argon at 7.5 $\mu A/cm^2$.

14. A: Dynamic POSSIMS spectrum in the bulk silver foil (type A sample, Table 2). B: Dynamic NEGSIMS spectrum in the bulk silver foil (type A sample, Table 2). Analysis conditions identical to those of Fig. 13.

15. AES depth profiles for silver surfaces reformed electrochemically under different solution conditions: A - deoxygenated aqueous KCl (type G sample, Table 2). B - air-saturated aqueous KCl (type H sample, Table 2) and C - oxygen-saturated KCl (type I sample, Table 2). Primary beam for AES was 1 KeV at 5 μA target current. Silver transition at 350 eV and chlorine transition at 180 eV were monitored. Sputtering conditions were argon at 1 KeV and 25 $\mu A/cm^2$ for all samples.

16. NEGSIMS depth profile of m/e = 24 and 26 across the reformed silver layer/bulk silver foil interface. Primary ion beam was 1 KeV argon at 500 $\mu A/cm^2$. The sample was of type G (Table 2) and had been sputtered for several hours prior to recording this profile.

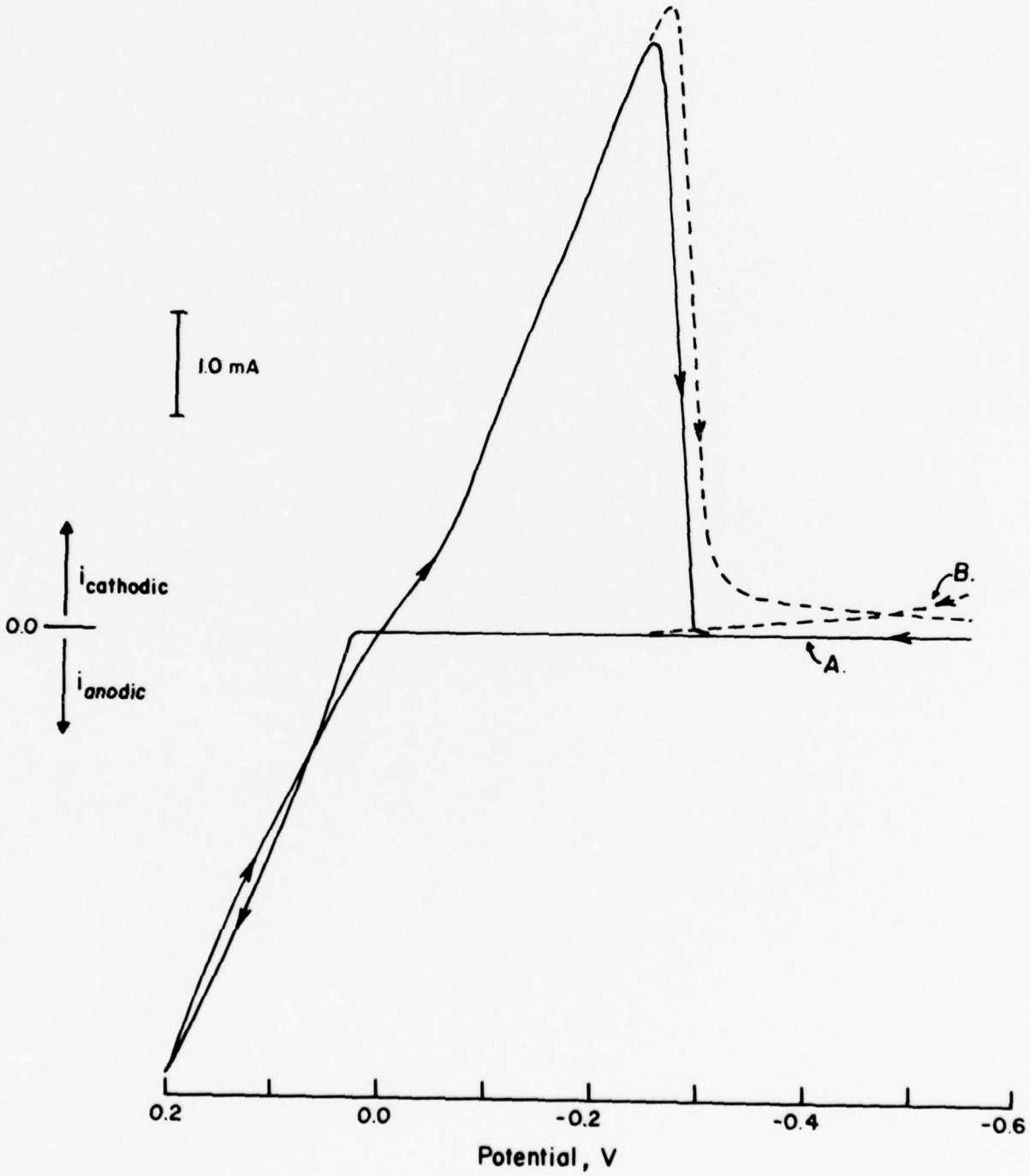
1.0 mA
i cathodic
0.0
i anodic
B.
A.
0.2
0.0
-0.2
-0.4
-0.6
Potential, V

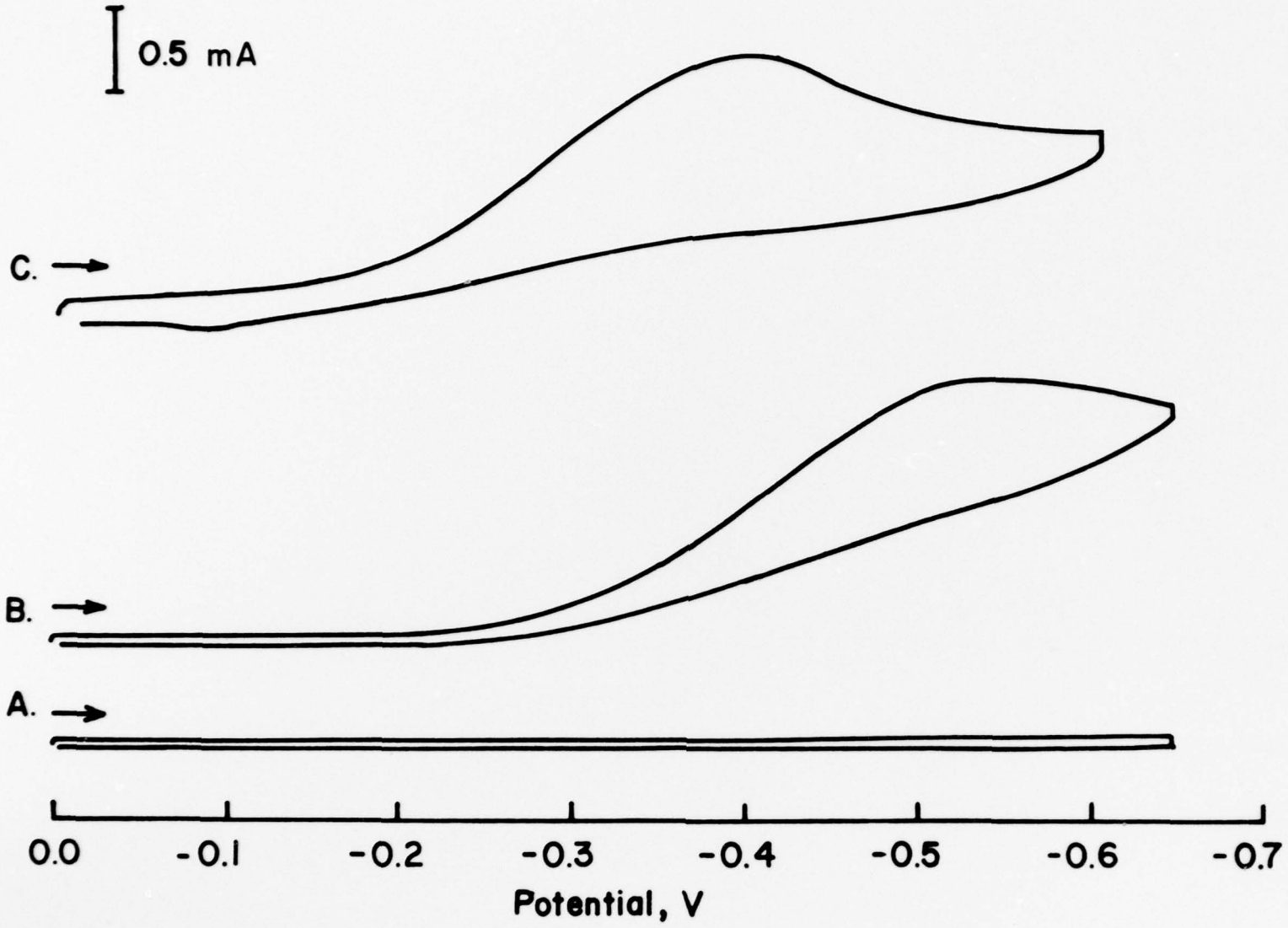
0.5 mA
C.
B.
A.
0.0
-0.1
-0.2
-0.3
-0.4
-0.5
-0.6
-0.7
Potential, V

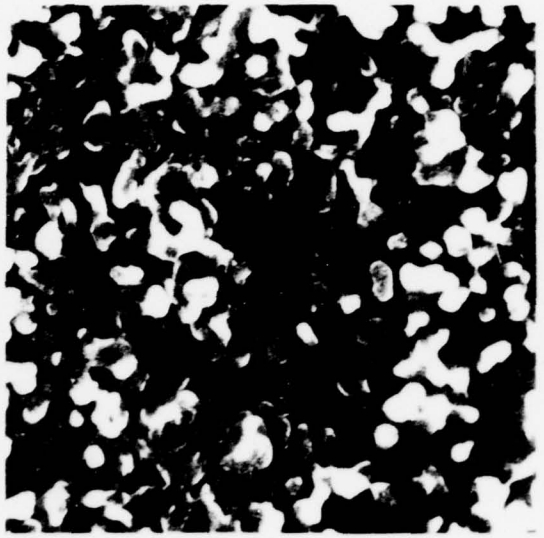

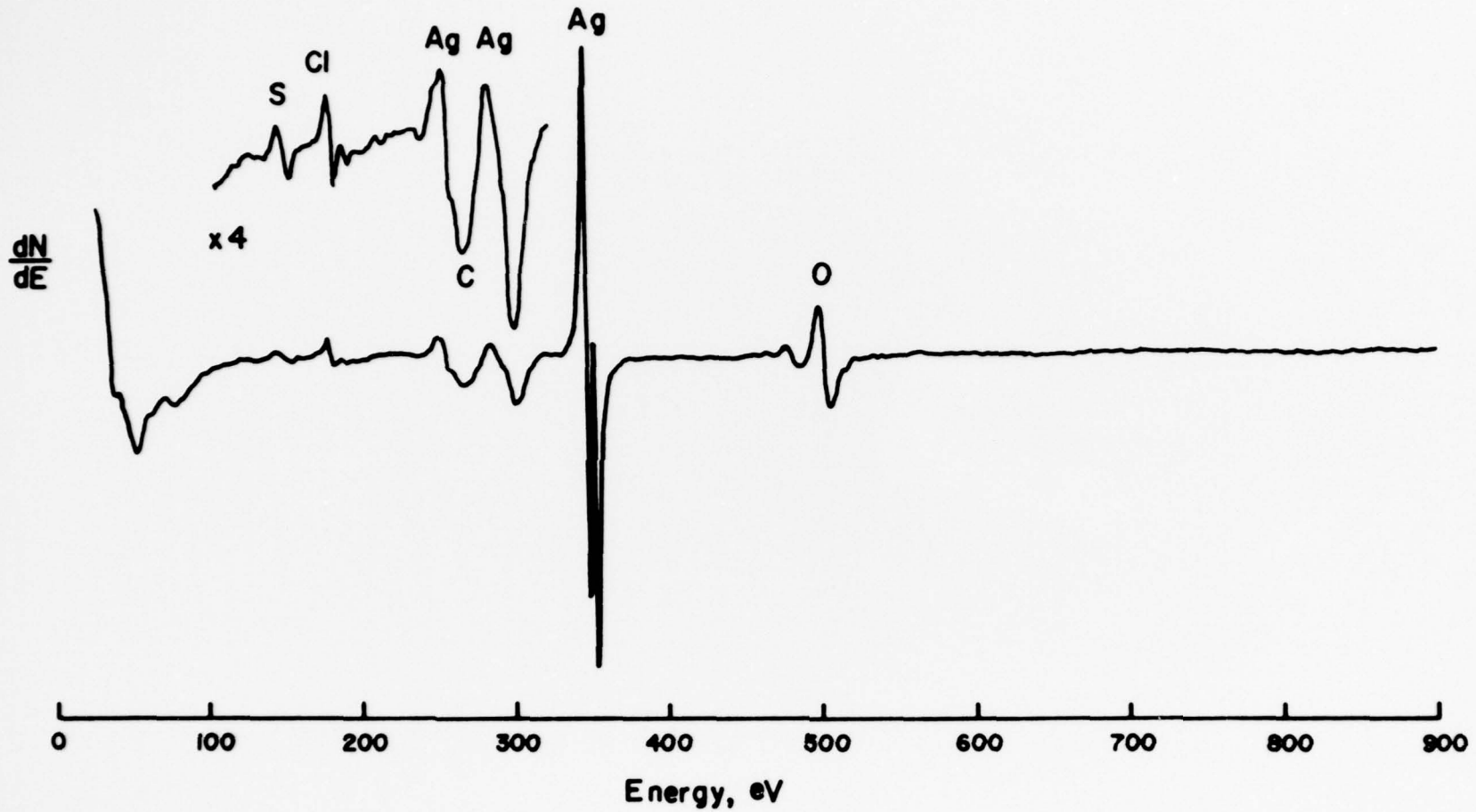
S
Cl
Ag
Ag
Ag
x4
C
O
dN/dE
0
100
200
300
400
500
600
700
800
900
Energy, eV

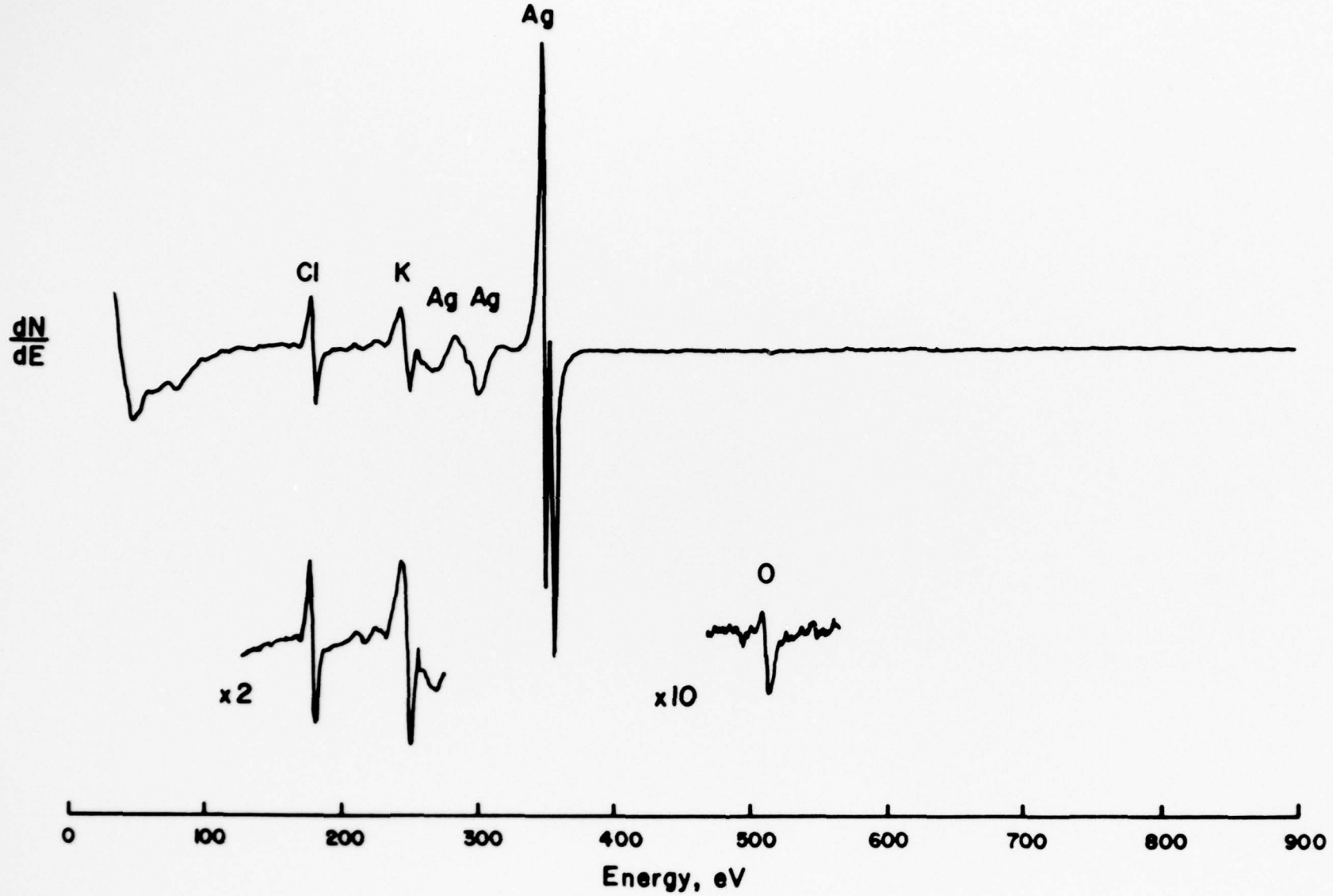
Ag
Cl
K
Ag
Ag
dN/dE
x2
O
x10
0
100
200
300
400
500
600
700
800
900
Energy, eV

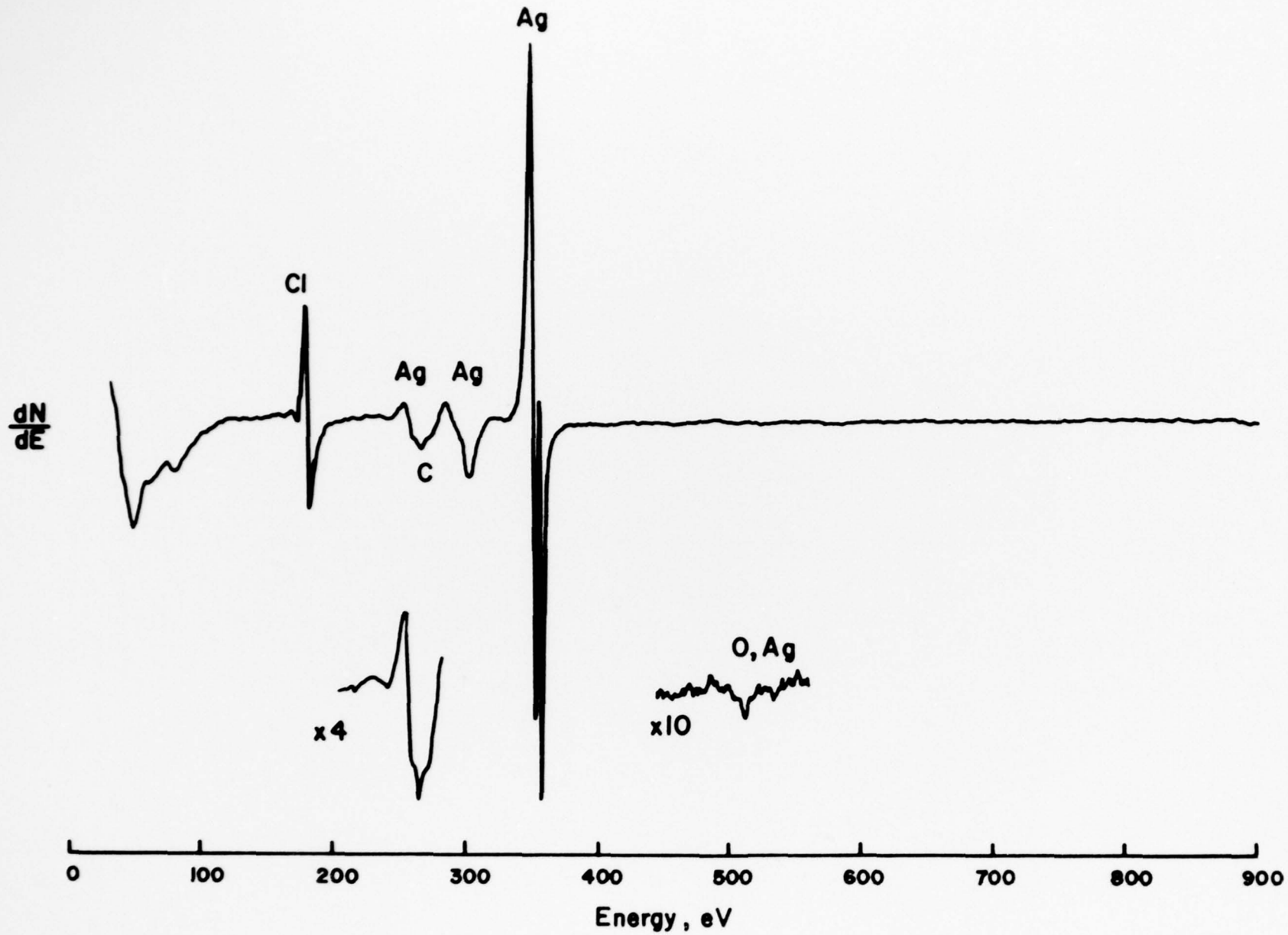
Ag
Cl
Ag
Ag
C
dN/dE
x4
O, Ag
x10
0
100
200
300
400
500
600
700
800
900
Energy, eV

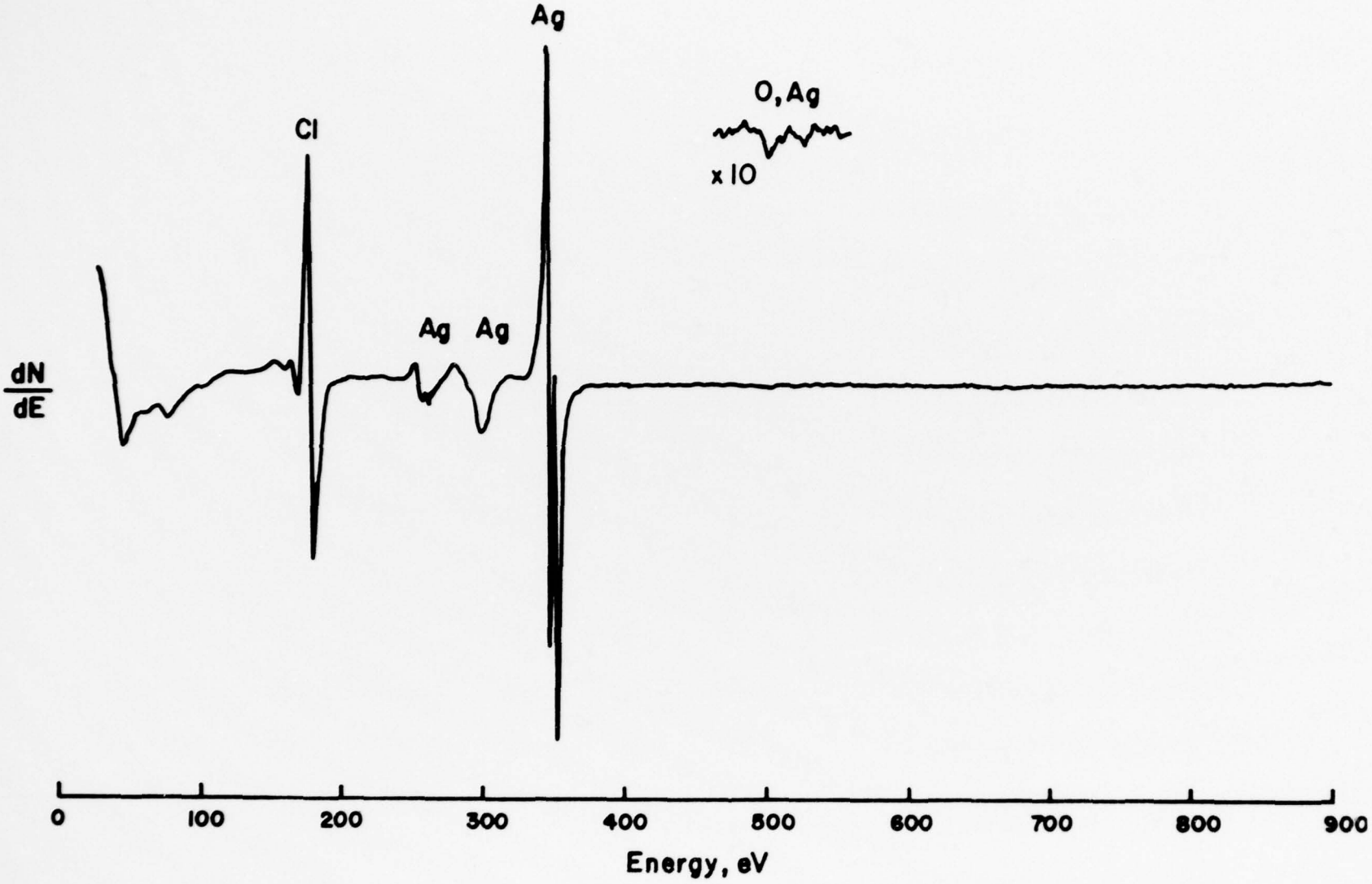
Ag
O, Ag
x 10
Cl
Ag
Ag
dN/dE
0
100
200
300
400
500
600
700
800
900
Energy, eV

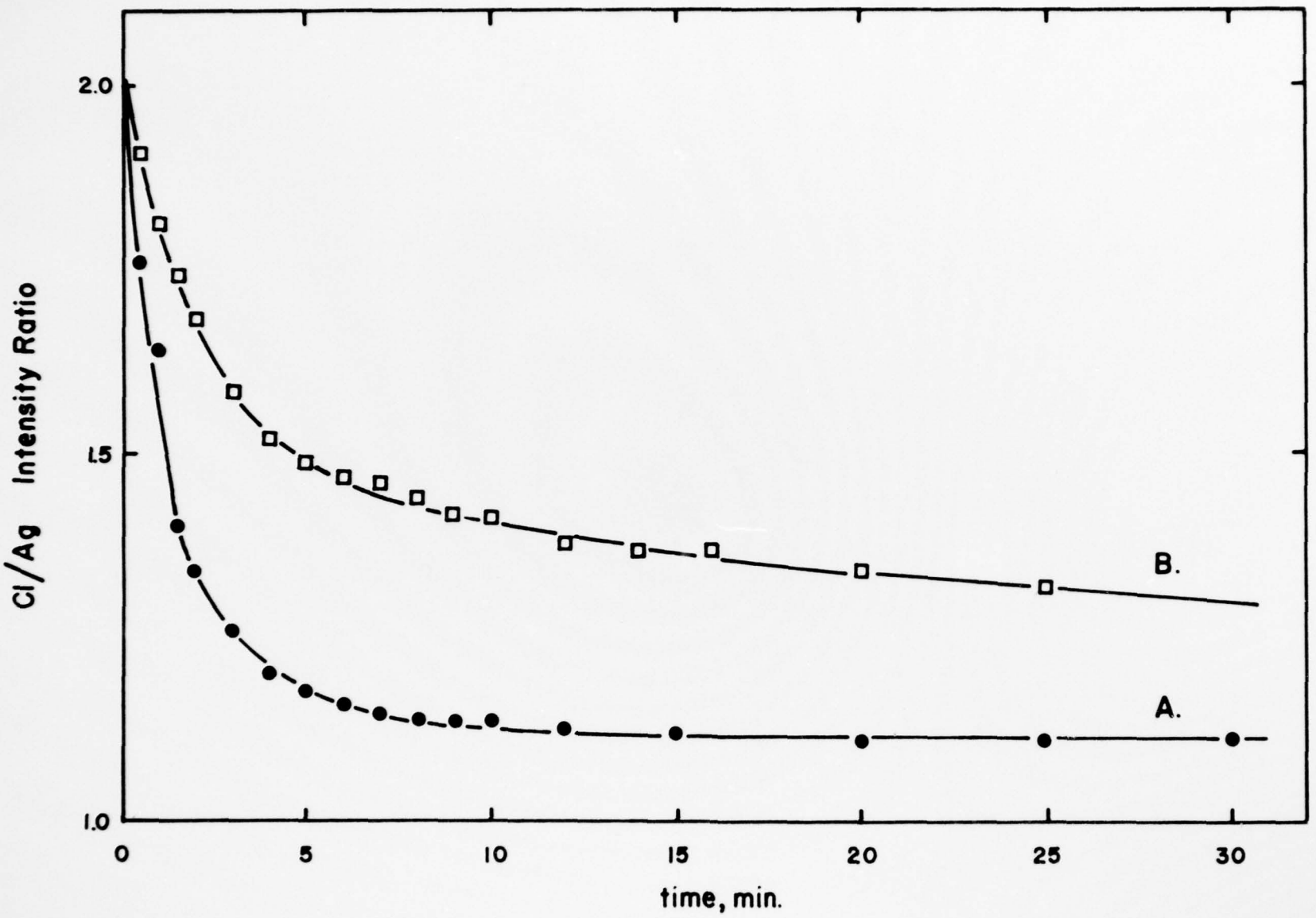
Cl/Ag Intensity Ratio
2.0
1.5
1.0
0
5
10
15
20
25
30
time, min.
B.
A.

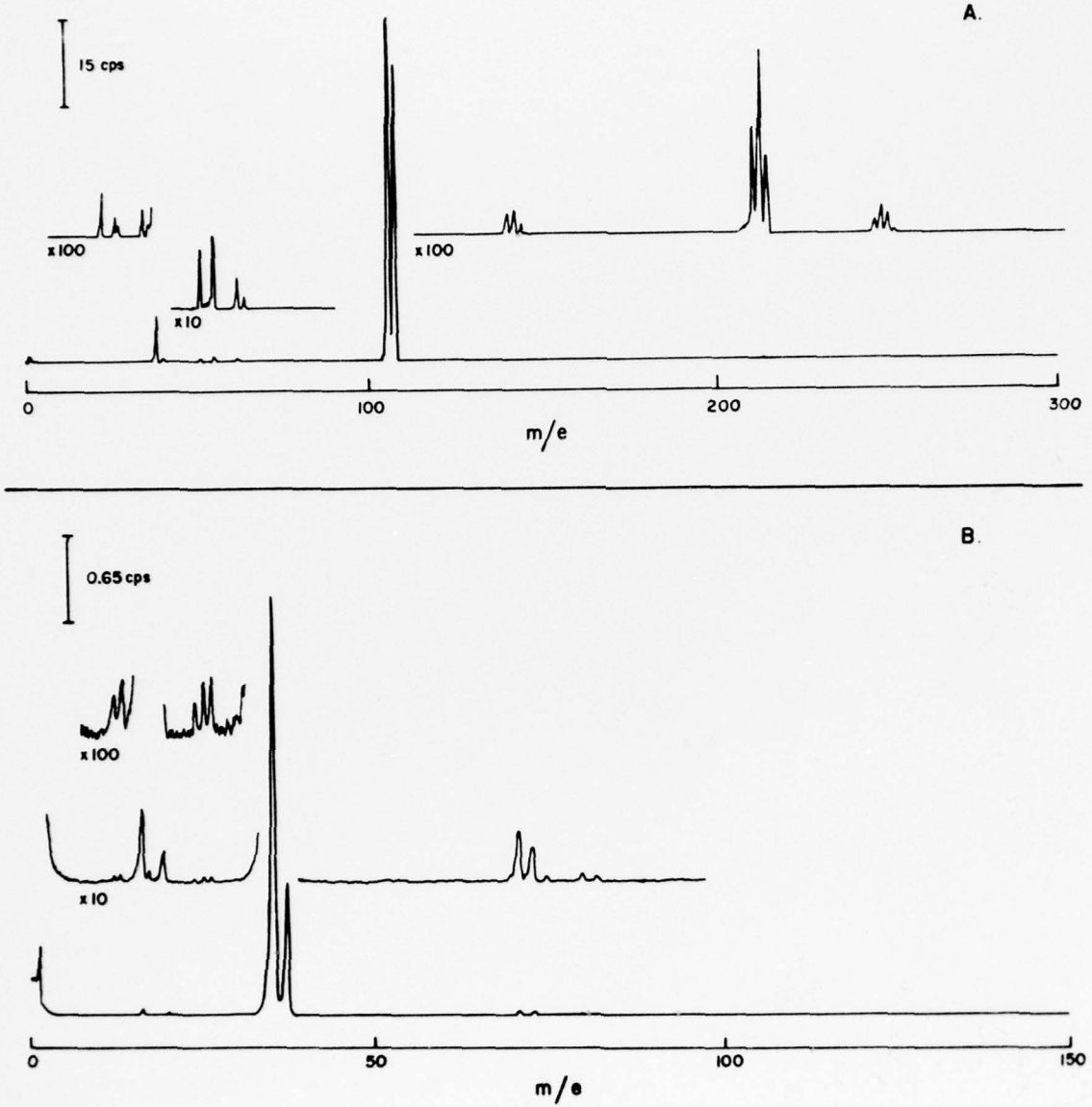
A.
15 cps
x100
x10
x100
0
100
200
300
m/e
B.
0.65 cps
x100
x10
0
50
100
150
m/e

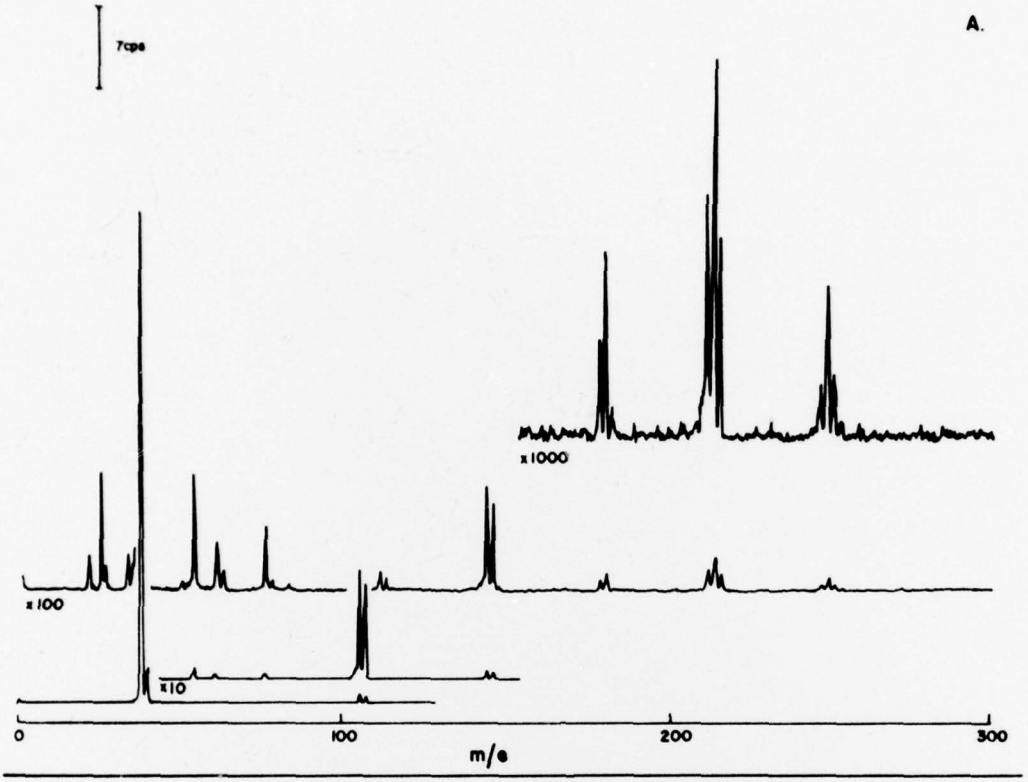
A.
7cps
x1000
x100
x10
0
100
200
300
m/e

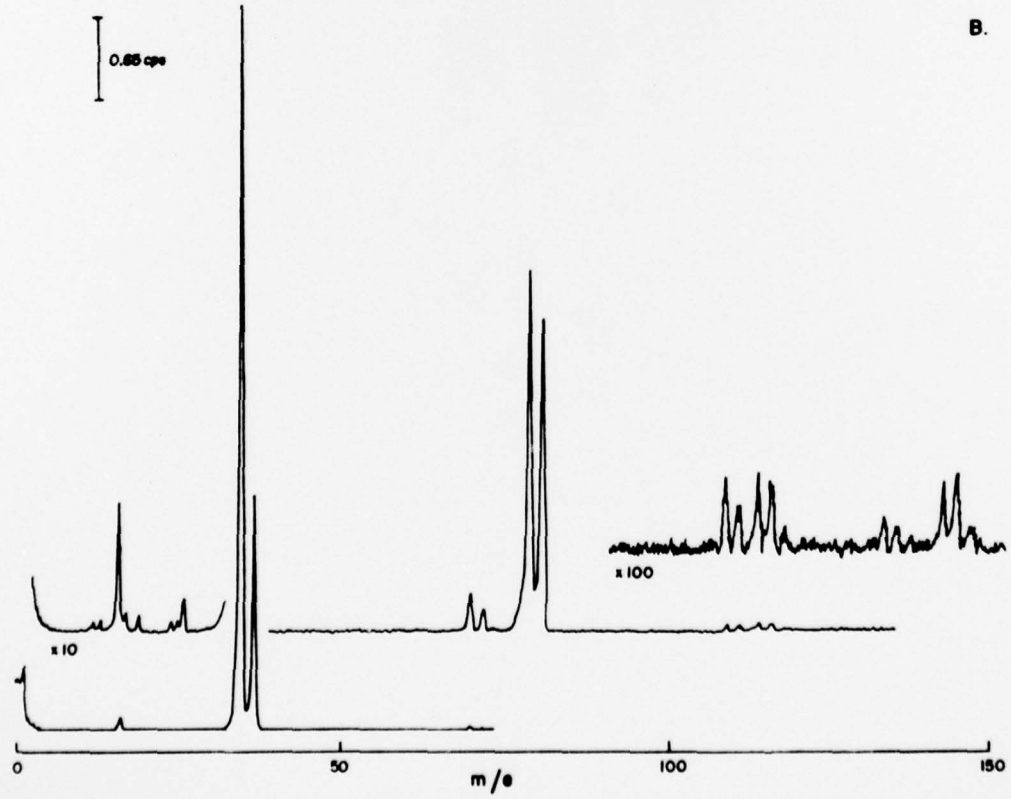
B.
0.65 cps
x100
x10
0
50
100
150
m/e

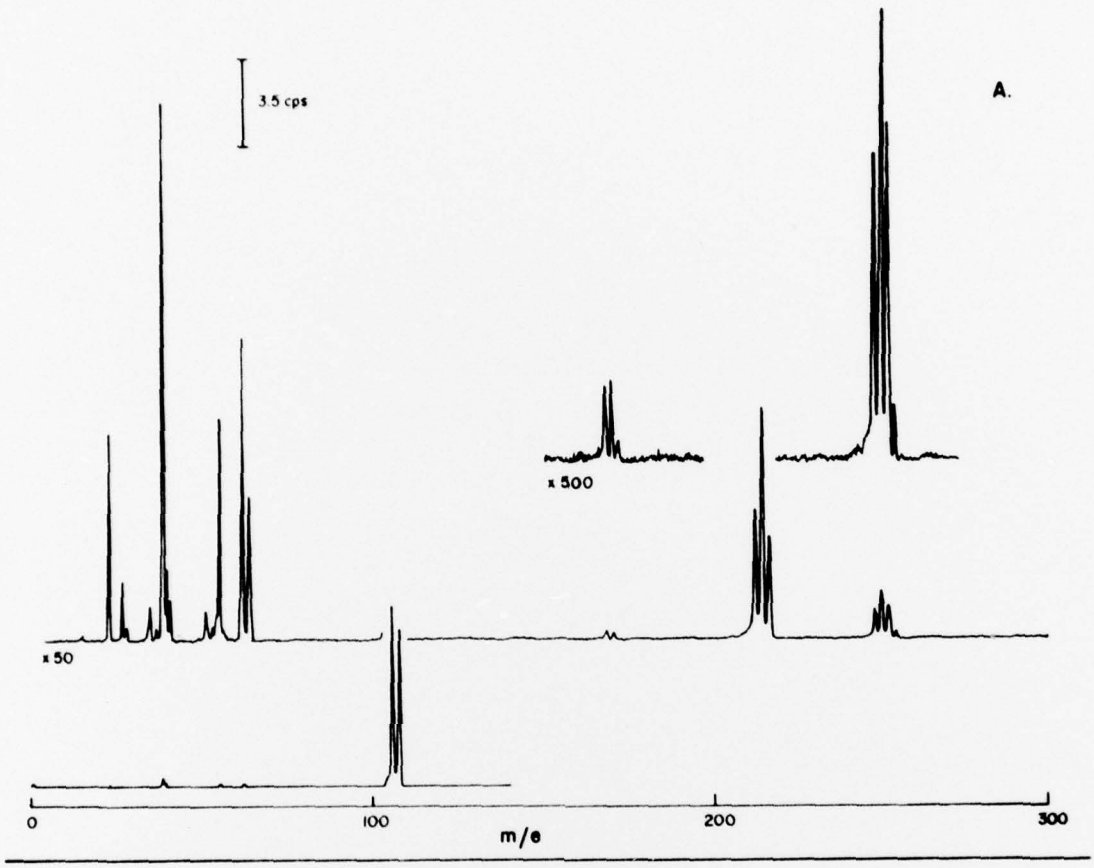
3.5 cps
A.
x 500
x 50
0
100
200
300
m/e

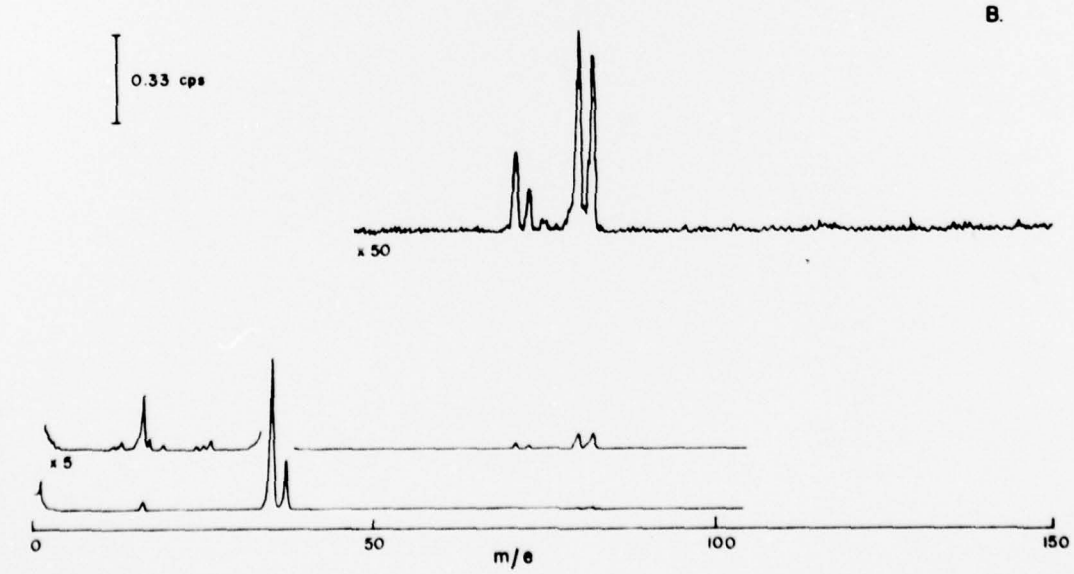
B.
0.33 cps
x 50
x 5
0
50
100
150
m/e

A. 0.5 μ

B. 10 μ

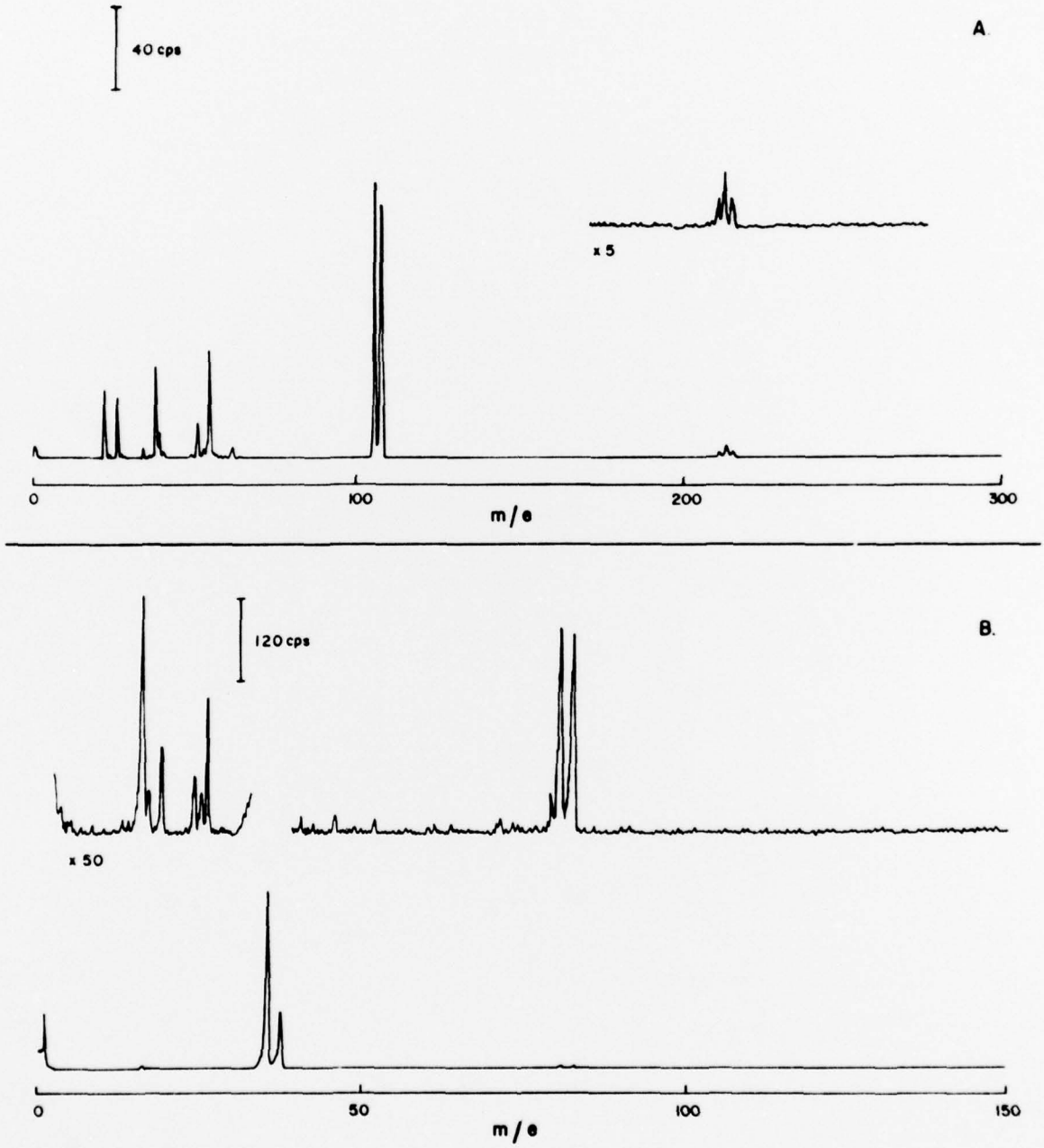
40 cps
A.
x 5
0
100
200
300
m/e
120 cps
B.
x 50
0
50
100
150
m/e

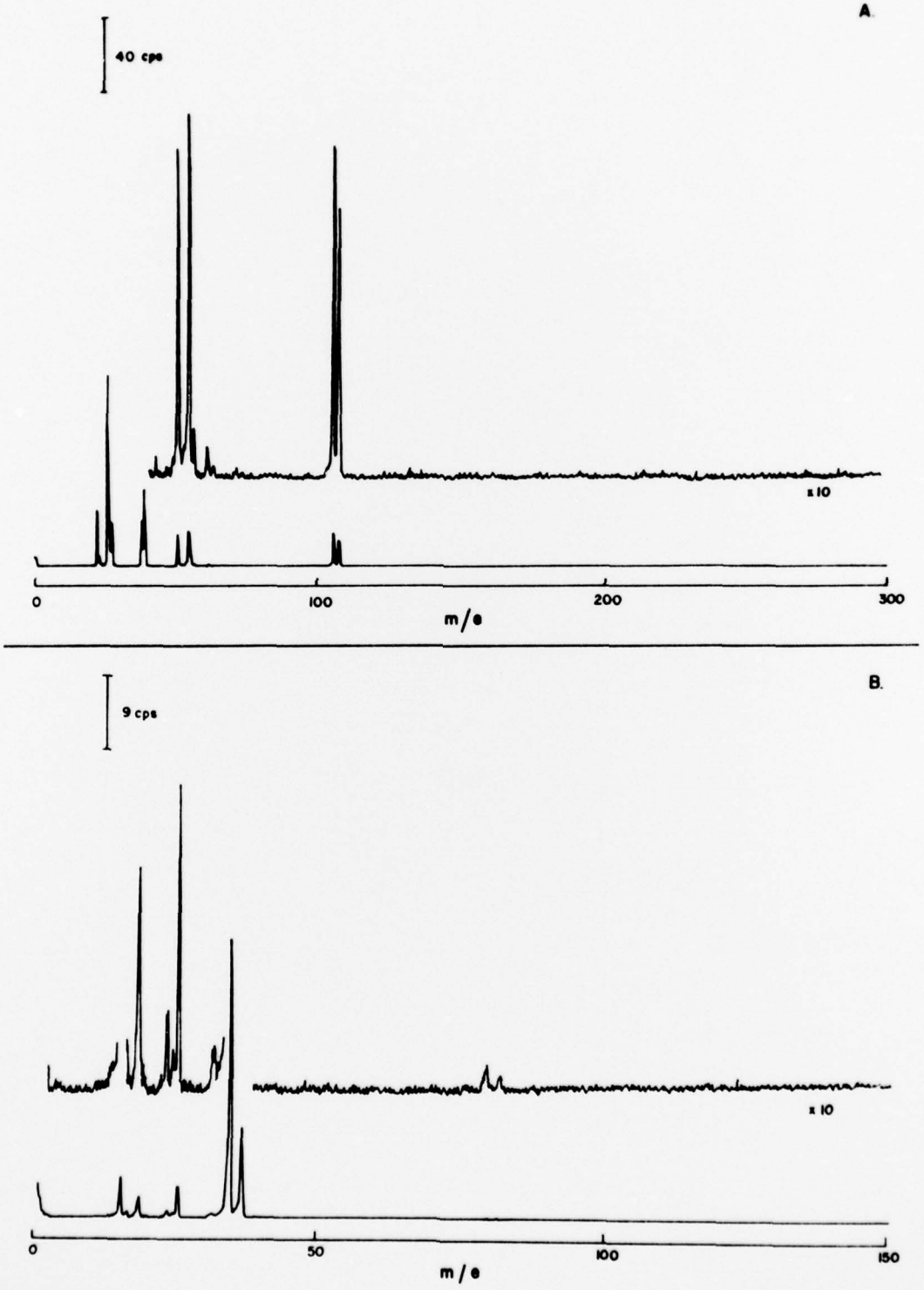
A.
40 cps
x 10
0
100
200
300
m/e
B.
9 cps
x 10
0
50
100
150
m/e

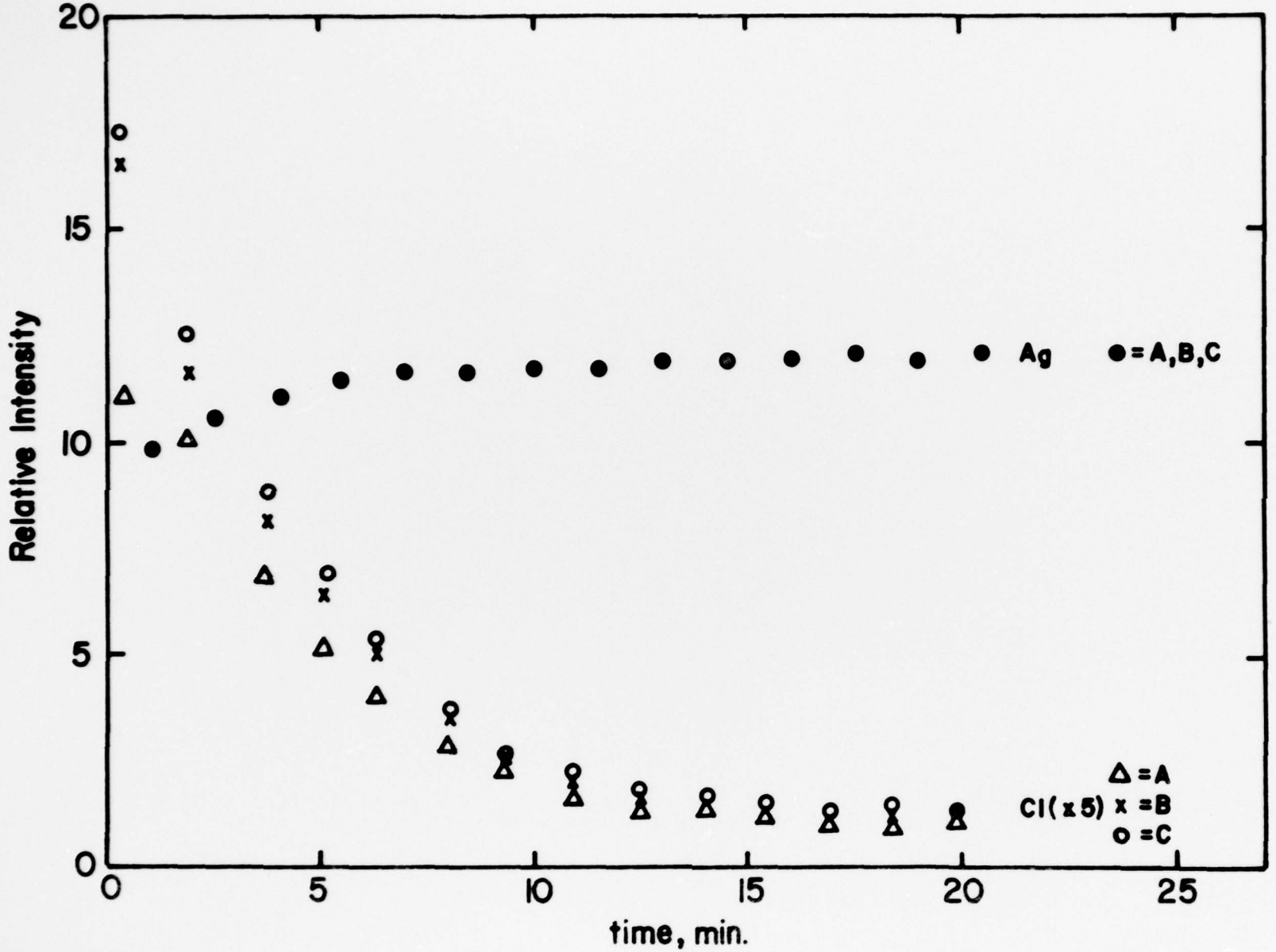
20
15
10
5
0
0
5
10
15
20
25
Relative Intensity
time, min.
Ag
●=A,B,C
△=A
Cl(x5) x=B
o=C

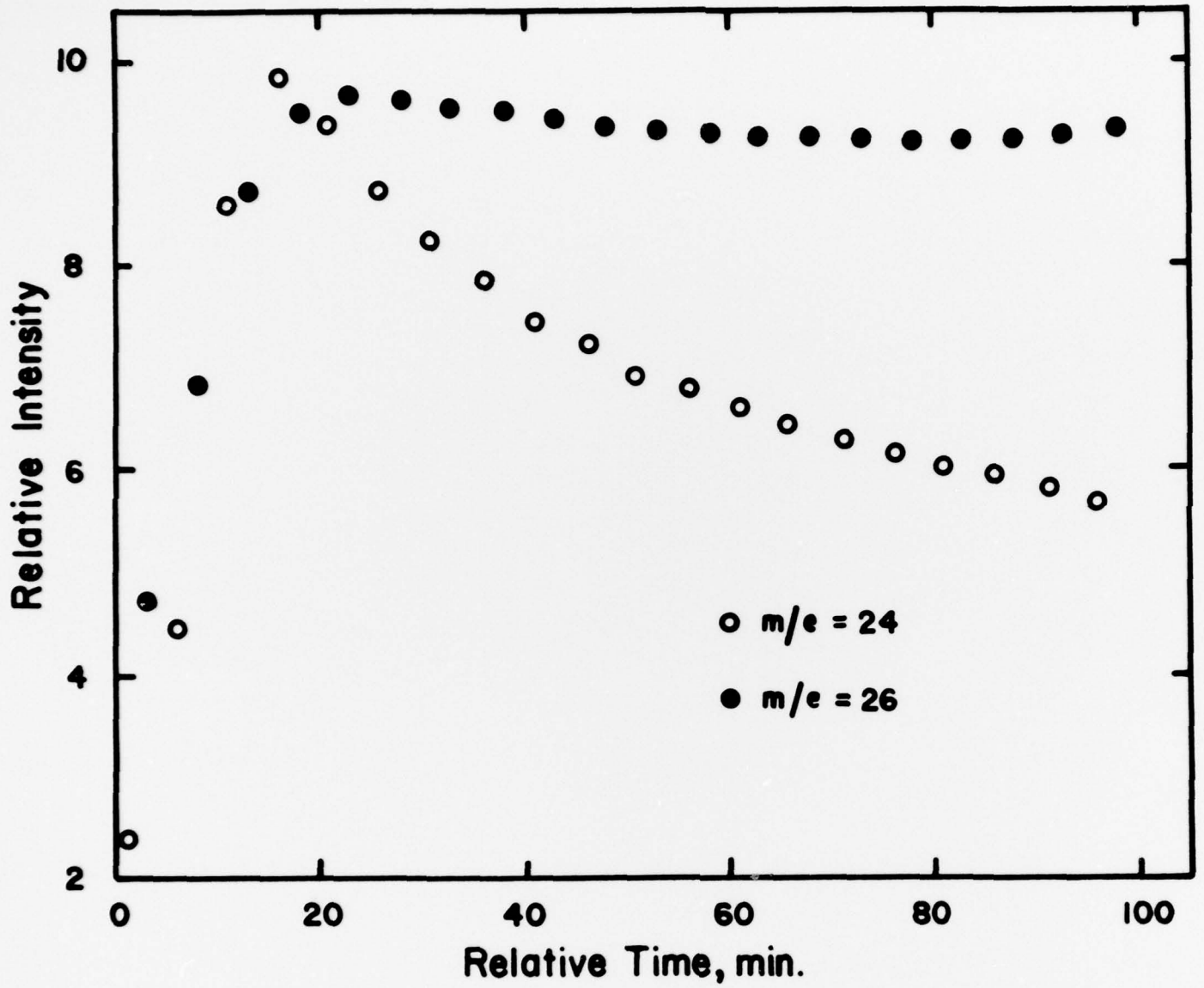
Relative Intensity
10
8
6
4
2
0
20
40
60
80
100
Relative Time, min.
m/e = 24
m/e = 26